SPRING / SUMMER 2026
VOLUME 18, NUMBER 1

Print ISSN: 2152-4157
Online ISSN: 2152-4165

WWW.IJERI.ORG

International Journal of Engineering Research & Innovation

Editor-in-Chief: Mark Rajai, Ph.D.
California State University Northridge

Published by the
International Association of Journals & Conferences

CUTTING EDGE JOURNAL OF RESEARCH AND INNOVATION IN ENGINEERING

www.ijeri.org

Print ISSN: 2152-4157
Online ISSN: 2152-4165

www.iajc.org

INTERNATIONAL JOURNAL OF ENGINEERING RESEARCH AND INNOVATION

ABOUT IJERI:

- IJERI is the second official journal of the International Association of Journals and Conferences (IAJC).
- IJERI is a high-quality, independent journal steered by a distinguished board of directors and supported by an international review board representing many well-known universities, colleges, and corporations in the U.S. and abroad.
- IJERI has an impact factor of **1.58**, placing it among an elite group of most-cited engineering journals worldwide.

OTHER IAJC JOURNALS:

- The International Journal of Modern Engineering (IJME) For more information visit www.ijme.us
- The Technology Interface International Journal (TIIJ) For more information visit www.tiij.org

IJERI SUBMISSIONS:

- Manuscripts should be sent electronically to the manuscript editor, Dr. Philip Weinsier, at philipw@bgsu.edu.

  For submission guidelines visit www.ijeri.org/submissions

TO JOIN THE REVIEW BOARD:

- Contact the chair of the International Review Board, Dr. Philip Weinsier, at philipw@bgsu.edu.

  For more information visit www.ijeri.org/editorial

INDEXING ORGANIZATIONS:

- IJERI is indexed by numerous agencies. For a complete listing, please visit us at www.ijeri.org.

Contact us:

Mark Rajai, Ph.D.

Editor-in-Chief
California State University-Northridge
College of Engineering and Computer Science
Room: JD 4510
Northridge, CA 91330
Office: (818) 677-5003
Email: mrajai@csun.edu

www.tiij.org

www.ijme.us

International Journal of Engineering Research and Innovation

The INTERNATIONAL JOURNAL OF ENGINEERING RESEARCH AND INNOVATION (IJERI) is an independent and not-for-profit publication, which aims to provide the engineering community with a resource and forum for scholarly expression and reflection.

IJERI is published twice annually (fall and spring issues) and includes peer-reviewed research articles, editorials, and commentary that contribute to our understanding of the issues, problems, and research associated with engineering and related fields. The journal encourages the submission of manuscripts from private, public, and academic sectors. The views expressed are those of the authors and do not necessarily reflect the opinions of the IJERI editors.

EDITORIAL OFFICE:

Philip D. Weinsier, Ed.D.
Manuscript Editor
Office: 419.372.0628
Email: philipw@bgsu.edu
Department of Applied Sciences
Bowling Green State University-Firelands
One University Dr.
Huron, OH 44839

The International Journal of Engineering Research and Innovation Editors

Table of Contents

In This Issue (p.25) Choose Your Reality

Philip Weinsier, IJERI Manuscript Editor

Just as men and women are groups within the category of humans but are notably different, and just as cars and trucks are groups within the category of vehicles but are notably different, so too are the groups of "realities" within the category of extended reality (XR). VR stands for virtual reality. In this type of reality, the user is immersed in a completely fake world. VR requires a full headset that blocks your vision of anything in the real world. What does the person wearing the headset see? Nowadays, the options are virtually (pun intended) limitless but could be anything from an entire movie theater built just for you, to a realistic first-person shooter video game, to virtual tourism. My personal favorite is virtual tourism, where viewers believe they are actually skiing in the Swiss Alps, sailing the high seas, or shopping in the Villaggio Mall in Doha, Qatar, which features Venetian architecture, cobblestone walkways, intricate façades, and an indoor canal where guests can take gondola rides under a painted sky ceiling.

Video games are arguably high on the list of VR applications. One of the most popular examples of VR is the metaverse. This is a collection of virtual digital worlds that a person can access via a VR headset. In metaverse environments, you can interact with other users' avatars, play games, buy virtual property, and more. Meta (formerly Facebook) is a major metaverse developer, though there are many other examples out there, such as Epic Games, Decentraland, Roblox, and Unity. Since VR can employ almost any kind of immersive experience the human mind can devise, business and industry have employed the technology for employee training, architecture, therapy, and educational videos.

AR stands for augmented reality. In this type of reality, you will still use computer-generated images. But, since the point is to also see your surroundings, the virtual elements are superimposed onto real-world items. Here, your physical environment is enhanced or changed in some way. AR can drastically change how we shop by letting us do all sorts of neat reality-bending tasks, such as trying on clothes, testing how furniture will fit in a room, and viewing customer ratings on top of in-store products. The most common AR applications for businesses are in mobile shopping apps. For example, you can use AR to see how a piece of furniture or art will look in your home—obviously, this is a two-way street, where customers can benefit from the shop-from-home experience we've become accustomed to, while increasing sales for businesses. But, here again, businesses and industry can also use AR internally for training (e.g., projecting assembly instructions onto a workspace or identifying different work tools), e-commerce, education, marketing, interior design, and product design.

MR stands for mixed reality. This type of reality has a good bit of overlap with AR in that both can be used on your smartphone, tablet, or laptop, both superimpose virtual elements onto real-world items, and neither requires any special or pro hardware. The difference is that MR goes a step further by integrating digital objects into the real world in a way that allows those objects to interact with physical surroundings. MR devices map the environment in order for virtual objects to interact with surfaces, obstacles, and user actions. For example, a virtual robot in MR could walk behind furniture or interact with real objects, creating a highly immersive experience. Applications can be found for video gaming, military training, medical training, product design, interior design, employee training, education, museums, and healthcare. For instance, BAE Systems, a security, aerospace, and naval contractor, managed to improve its battery production rate by 30-40% using MR. Case Western Reserve in Ohio used MR to teach anatomy. In this case, students used Microsoft HoloLens 2 to visualize a virtual human skeleton and its inner anatomy, thereby allowing them to get an in-depth look at an un-dissected cardiac system.

This brings us to our featured article (p.25) and an educational application of AR. The authors designed, built, and installed an interactive AR station to improve public awareness of invasive beetle species. The system combined a physical dodecahedron structure with interactive AR visualizations created in Unity, a real-time 3D development engine. Each face of the dodecahedron displayed information about different invasive species, while allowing users to scan the panels to view 3D beetle models and animations in AR. The goal of this project was to demonstrate that combining physical exhibits with AR content can create accessible and immersive learning experiences in visitor centers and educational environments. The aim of this approach was to make scientific topics, such as invasive species, more understandable and engaging for the general public.

Editorial Review Board Members

Scanning Electron Microscopy Validation for Additively Manufactured Stainless-Steel Cellular Bone Scaffolding

Mohammad O. Al-Barqawi, CHA Consulting; Mustafa Mahamid, University of Illinois-Chicago;
Adeeb Rahman, University of Wisconsin-Milwaukee

Abstract

Additive manufacturing (AM) enables the fabrication of bone scaffolds with tailored mechanical properties to address stress shielding in orthopedic implants. In this study, stainless steel (SS316L) scaffolds with cubic and diagonal architectures were optimized to achieve an elastic modulus of 15 GPa, comparable to human cortical bone, and fabricated using laser powder bed fusion (LPBF). Compression testing confirmed the finite element predictions, yielding moduli of 14.76 GPa (cubic) and 14.29 GPa (diagonal). Scanning electron microscopy (SEM) demonstrated high structural fidelity with minimal porosity, though a 3-5% reduction in strut size was observed. Cubic scaffolds exhibited stretch-dominated failure suitable for load bearing, while diagonal scaffolds displayed bending-dominated failure favorable for energy absorption. These results demonstrated the feasibility of using LPBF to produce patient-specific SS316L scaffolds that minimize stiffness mismatch, promote bone ingrowth, and support long-term implant success.

Keywords: Additive Manufacturing; Laser Powder Bed Fusion; Bone Scaffold; Stress Shielding; Finite Element Analysis; Scanning Electron Microscopy; Orthopedic Implants

Introduction

Critical-sized bone defects present a major clinical challenge in orthopedics, requiring effective strategies for bone regeneration and mechanical support. Current treatments such as autografts and allografts face significant limitations, including restricted availability, donor site morbidity, and risks of immune rejection or disease transmission (Ponader et al., 2010; Li, Habibovic, van den Doel, Wilson, de Wijn, van Blitterswijk & de Groot, 2007). These challenges have motivated the development of synthetic bone scaffolds capable of providing both structural stability and biological guidance for tissue regeneration. A crucial consideration in scaffold design is the prevention of stress shielding, which arises when an implant's stiffness substantially exceeds that of natural bone (10-20 GPa). This mismatch causes the implant to bear most of the mechanical load, reducing stress on surrounding bone tissue and leading to resorption, loosening, and eventual implant failure (Öhman, Baleani, Pani, Taddei, Alberghini, Viceconti & Manfrini, 2011). Current metallic implants often possess much higher stiffness than bone, highlighting an important research gap in developing materials that match bone's elastic properties while maintaining sufficient strength and porosity to support biological integration (Lin, Kikuchi & Hollister, 2004; Karageorgiou & Kaplan, 2005). Recent studies have also shown that lattice architecture strongly influences mechanical behavior, with stretch- and bending-dominated unit cells exhibiting distinct structural responses (Maskery, Aboulkhair, Aremu, Tuck, Ashcroft, Wildman & Hague, 2016; Abou-Ali, Al-Ketan, Rowshan & Abu Al-Rub, 2019; Kadkhodapour, Montazerian, Darabi, Anaraki, Ahmadi, Zadpoor & Schmauder, 2015).

This study addresses this gap by employing laser powder bed fusion (LPBF) to fabricate scaffolds from stainless steel 316L (SS316L). This alloy was selected due to its excellent corrosion resistance, biocompatibility, and cost-effectiveness compared to titanium alloys, as well as its favorable performance in AM processes (Kurzynowski, Gruber, Stopyra, Kuźnicka & Chlebus, 2018; Rankouhi, Bertsch, Meric de Bellefon, Thevamaran, Thoma & Suresh, 2020). The authors hypothesized that specific cellular architecture—cubic and diagonal unit cells—could be optimized to achieve mechanical properties consistent with natural cortical bone, particularly an elastic modulus of approximately 15 GPa. The authors integrated finite element analysis (FEA) to optimize scaffold geometry with experimental validation through compression testing and scanning electron microscopy (SEM). The investigation focused on the ability of optimized cubic and diagonal designs to achieve bone-like stiffness while maintaining porosity for tissue ingrowth (Asadi-Eydivand, Solati-Hashjin, Fathi, Padashi & Abu Osman, 2016; Al-Ketan, Rowshan & Abu Al-Rub, 2018; Ma, Zhang, Zhao, Jiang, Luo & Zhou, 2022). Figure shows that, following LPBF fabrication, scaffolds underwent morphological evaluation to assess structural fidelity, surface roughness, and manufacturing accuracy.

Overall, this work demonstrated that architectural design can significantly influence scaffold behavior, with cubic scaffolds showing stretch-dominated failure modes suitable for load-bearing applications and diagonal scaffolds exhibiting bending-dominated failure favorable for energy absorption. Establishing these structure–property relationships provides valuable insights for minimizing stress shielding and advancing patient-specific scaffold design, thereby contributing to improved bone integration and long-term orthopedic implant success (DebRoy et al., 2018; Lewandowski & Seifi, 2016).

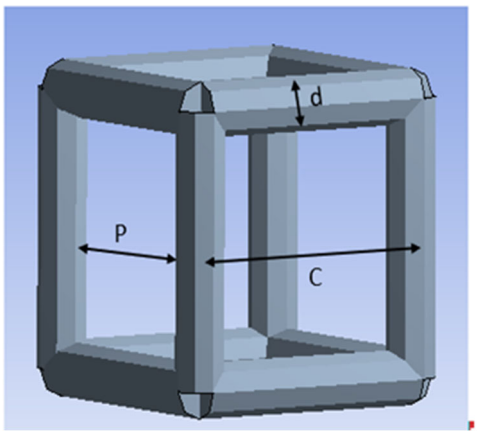

(a) Cubic

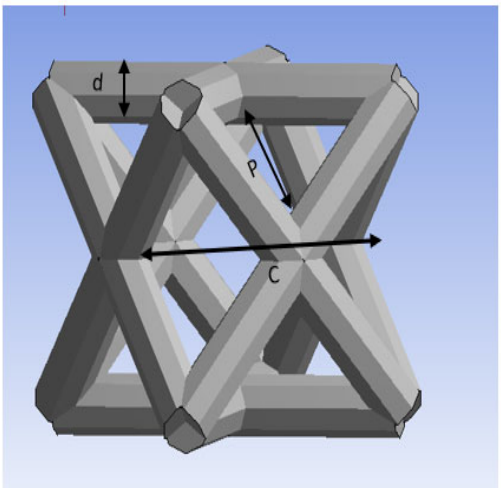

(b) Diagonal

Figure 1. Unit cells.

Material and Methods

Stainless steel (SS316L), a widely used material for bone tissue engineering (BTE) scaffolds and additive manufacturing, was selected for this study owing to its superior biocompatibility, established corrosion resistance in physiological environments, and favorable combination of mechanical properties and cost-effectiveness relative to titanium alloys. Mechanical property variations, stemming from process parameters, build orientation, and inherent material properties, necessitated characterization via tensile testing. Tensile coupons were additively manufactured and tested at room temperature using an MTS tensile machine equipped with a 50 KN load cell. Digital image correlation (DIC) was utilized to measure strain. DIC, a non-contact optical method, tracks the displacement of a random speckle pattern applied to the specimen surface during loading. By analyzing sequential high-resolution images, DIC produces full-field displacement and strain maps with sub-pixel precision, thereby minimizing errors commonly associated with traditional extensometers and providing a more comprehensive characterization of strain distribution, including localized concentrations that point-based techniques may fail to capture, resulting in stress-strain curves that provide values for elastic modulus, yield strength, ultimate strength, and elongation (Novich, Sánchez, Paniagua & Mantell, 2024).

Finite Element Analysis

FEA simulations were conducted in ANSYS to model the geometry and predict the mechanical behavior of BTE scaffolds under uniaxial compression. The two-unit cell designs used in this study were cubic and diagonal The cubic design represented a stretch-dominated lattice in which struts primarily carry axial loads, resulting in high relative stiffness and strength, making it well suited for load-bearing applications (Maskery et al., 2016; Al-Ketan et al., 2018). In contrast, the diagonal design was bending-dominated, exhibiting greater energy absorption capacity and a more compliant response (Zhu, Li, Wang, Li, Hou, Hao, Yang & Misra, 2019). Such mechanical behavior contributes to reducing stress shielding and facilitates bone remodeling by more closely replicating the native mechanical environment of bone. The two cell units were parameterized for cell size (c), strut size (d), and pore size (p). Pore size was fixed at 800 μm to accommodate bone ingrowth, as established in prior studies (Taniguchi et al., 2016; Wang, Xu, Li, Yi, Zhang, He & Yu, 2020). Optimization tools in ANSYS adjusted geometrical parameters to achieve a scaffold elastic modulus of 15 GPa.

The relationship between the geometrical parameters c, d, and p is given through the following equations. For the cubic unit cell (Equation 1) and the diagonal unit cell (Equation 2):

$$p = c - d \tag{1}$$

$$p = \sqrt{2} * \left(\frac{c}{2} - d \right) \tag{2}$$

In this study, both 3x3 and 7x7 scaffolds were explored. Figures 2 and 3 show the final geometry of the 3x3 cubic and diagonal scaffolds, respectively. The strut size and the basic cell size were limited within a specific range according to the capability of the AM technology used in this research study.

Additive Manufacturing

The optimized designs were fabricated using LPBF technique on an EOS M290 machine. The STL file format facilitated compatibility with 3D prototyping. Table 1 details the LPBF processing parameters. The process included layer-by

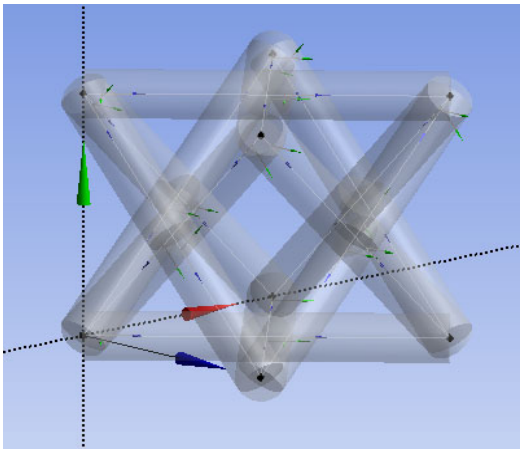

Figure 2. Diagonal unit cell.

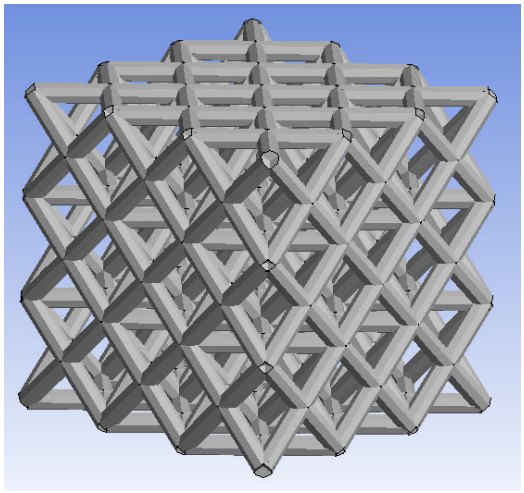

(a) Diagonal

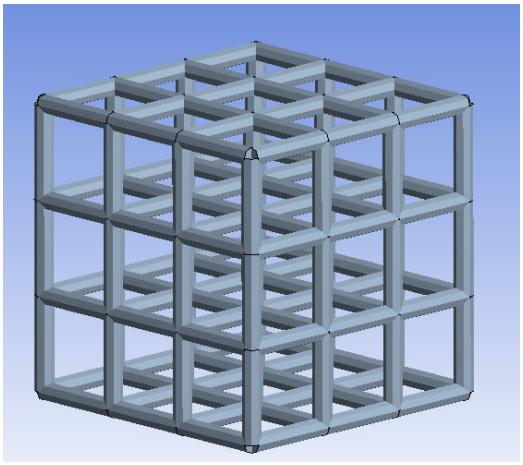

(b) Cubic

Figure 3. BTE scaffold.

-layer powder deposition, laser fusion, and eventual removal of scaffolds via electrical discharge machining (EDM). Scaffold support structures were integrated during printing to ensure stability. AM technology was used to construct the BTE scaffold with high precision. Figure 4 shows the final design that was saved in the STL file format, which is compatible with all 3D prototyping machines. The AM process used to construct the SS316L BTE scaffold was LPBF. Figure 5 shows examples of precision-manufactured cellular structures produced by a machine such as the EOS M290. Table 1 shows the processing parameters used to build the scaffolds.

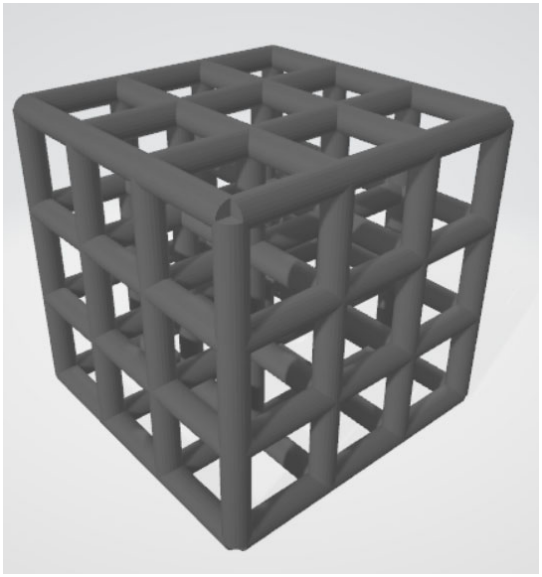

(a) Cubic

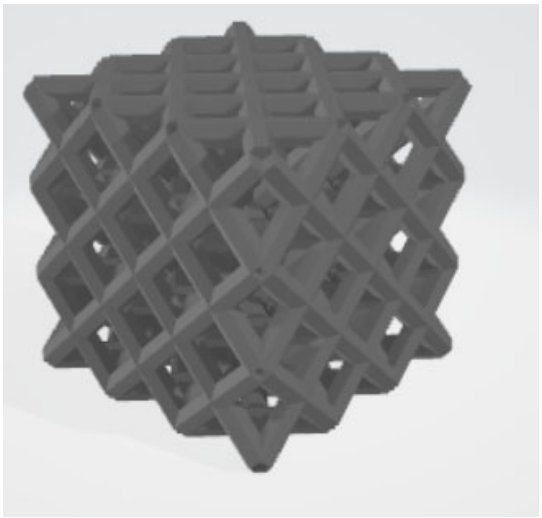

(b) Diagonal

Figure 4. Scaffolds in STL format.

Figure 5. Examples of precision-manufactured cellular structures.

Table 1. LPBF processing parameters.

Processing parameter	Value
Build direction	30 - 45^{o} angles
Laser power: Infill	195 W
Laser power: Contour	110 W
Laser speed: Infill	1083 mm/s
Laser speed: Contour	800 mm/s
Infill rate	100%
Layer thickness	200 microns
Platform temperature	80^{o}C

The primary advantages of using LPBF are the ability to construct scaffolds with complex internal and external structures and build scaffolds in one process with an absence of tooling and with the capability of building scaffolds with varying wall sections to achieve optimized mechanical properties (Murr et al., 2010). LPBF is considered a costly process, as it requires a significant amount of energy, considering material and post-processing costs (DebRoy et al., 2018). The following is a step-by-step explanation of the LPBF material processing methodology.

1. A recoating blade is used to deposit a layer of powder (around 20 microns) on the build platform via laser, which heats the bottom layer of powder locally.
2. The build platform moves one layer down, and the recoating blade moves by a roller and deposits the second layer of powder on the building platform.
3. The second layer of powder is fused to the first layer.
4. Steps 2 and 3 are repeated until the scaffold is built completely.
5. The powder is removed from the building platform once the final layer has been constructed.
6. Electrical discharge machining (EDM) is used to remove the scaffold from the build plate.

The build plate size is 250 mm x 250 mm; hence the need for multiple CAD models to support it at the desired angle. The chamber in which printing is conducted was under vacuum to prevent SS oxidation while printing. The size of the SS316L powder particle used was less than 60 microns. Since the minimum angle required for SS to remain self-supporting is 30 degrees, the scaffolds were built with an angle of 30-45 degrees to prevent collapse during printing. SS support was added to the CAD model to support it at the desired angle. EDM was used to remove the support material from the scaffold. Figure 6 shows 3D printed cubic and diagonal scaffolds on the build plate with a support structure. Figure 7 depicts the 3D-printed scaffolds using LPBF after removal of support material and build plate.

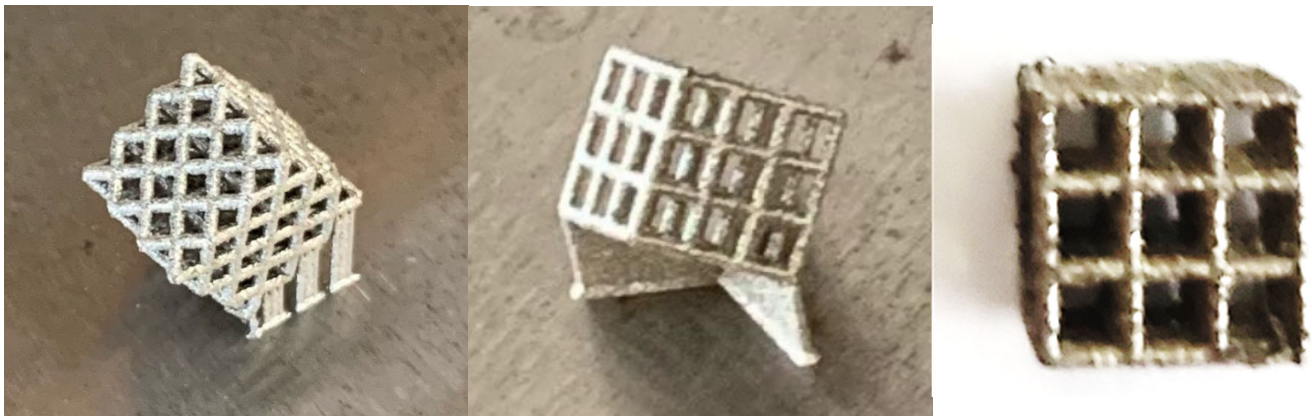

(a) Diagonal (b) Cubic (c) Cubic

Figure 6. Oriented 3D printed SS scaffolds with support structure.

Figure 7. 3D printed scaffolds using LPBF after removal of support material and build plate.

Results and Discussion

Table 2 outlines the optimized geometrical parameters targeting cortical bone modules; Figure 8 shows an example of a generated diagonal cellular structure using this optimization. Morphological characterization via SEM and microscopy revealed well-fused powder particles, minimal porosity, and surface roughness. Variations in strut and cell sizes, likely due to AM limitations, introduced discrepancies between CAD models and manufactured scaffolds. Furthermore, energy-dispersive X-ray spectroscopy analysis confirmed the material composition to be primarily Fe, Cr, and Ni, consistent with SS316L specifications; no significant contamination was detected.

The surface roughness observed, a common feature of LPBF processes, had dual implications for clinical performance. A moderate degree of microroughness is generally beneficial for osteointegration, as it increases the surface area available for protein adsorption and osteoblast attachment, thereby promoting stronger bone–implant fixation. In contrast, excessive roughness can act as a nucleation site for fatigue cracks under cyclic physiological loading, ultimately reducing the long-term mechanical reliability of the scaffold (Leuders, Thöne, Riemer, Niendorf, Tröster, Richard & Maier, 2013; Masuo, Tanaka, Morokoshi, Yagura, Uchida, Yamamoto & Murakami, 2018). In addition, pronounced surface asperities may induce local stress concentrations in the surrounding bone tissue, potentially affecting implant stability.

Table 2. Geometrical parameters of the optimized BTE scaffolds.

Unit cell type	Pore size (micron)	Cell size (micron)	Strut size (micron)
Cubic	798	1059	646
Diagonal	812	2616	734

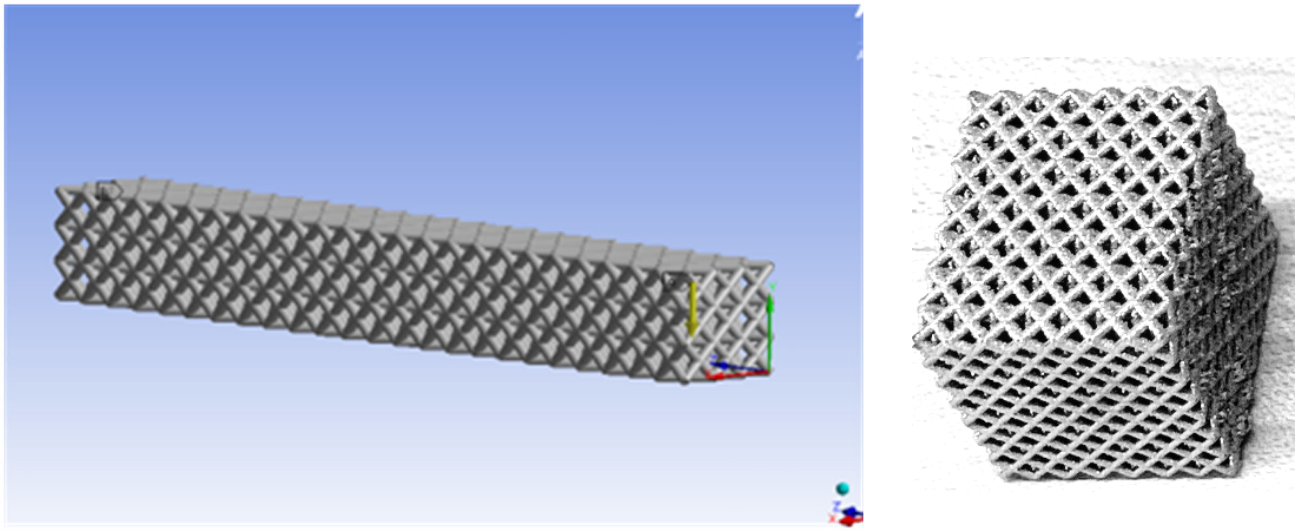

Figure 8. Example of a generated diagonal cellular structure using optimization.

The measured strut diameter deviations, approximately 3-5% lower than the nominal design, together with minor irregularities, were consistent with the dimensional tolerances typically reported for metal AM components (DebRoy et al., 2018; Masuo et al., 2018). These variations introduce only a minor and predictable discrepancy between experimental and FEA-derived mechanical properties, and the low variability in relative density confirms the reliability of the EOS M290 process. Importantly, the resulting mechanical properties remained within the modulus range of cortical bone, indicating that such deviations are acceptable for preclinical evaluation. For clinical translation, however, stricter process control and post-build metrology will be essential in ensuring that tolerances remain within a defined range to mitigate potential fatigue-related risks (Leuders et al., 2013).

SEM techniques utilizing both standard and stereoscopic microscopes were used to characterize the samples and evaluate the quality of the LPBF technique used to manufacture the scaffolds. Before imaging, the sample was mounted in clear epoxy with the face of the lattice facing the polishing surface. Next, the sample was polished into approximately half the thickness of the statues. Finally, the polishing procedure was accomplished using 800-1200-0.5 micron vibratory imaging. The sample was then mounted in clear epoxy with the face of the lattice facing the polishing surface. Next, the sample was polished into approximately half the thickness of the statues. Finally, the polishing procedure was accomplished using 800-1200-0.5 micron vibratory.

Figures 9 and 10 show images from standard and stereo microscopes. The stainless-steel powder particles were observed to be very well infused, as minimal porosity existed within the solid struts, which showed the effectiveness of the LPBF technique in manufacturing such samples. Rough surfaces and edges were noticed, which might create stress concentration issues at irregular surfaces while testing. In addition, the cross-sectional area of the struts was not constant throughout the scaffold.

The area varied within a specific range that depended on the input parameters used in the AM process. SEM was used to measure some of the struts' diameter and basic cell sizes. Figure 10 shows SEM images of the cubic and diagonal scaffolds. The struts sizes ranged between 597-638 microns for the cubic scaffold and 692-726 microns for the diagonal scaffold. The cell size was measured and found to be around 1439 microns and 2610 microns in both orthogonal directions for the cubic and diagonal scaffolds, respectively, which were very close to the target cell sizes achieved through optimization. However, the average strut sizes for the cubic and diagonal specimens were 3-5% lower than the optimized strut diameter, hence creating variations in structure relative densities between the CAD file and the manufactured scaffolds. In this sense, then, a discrepancy in the results was expected.

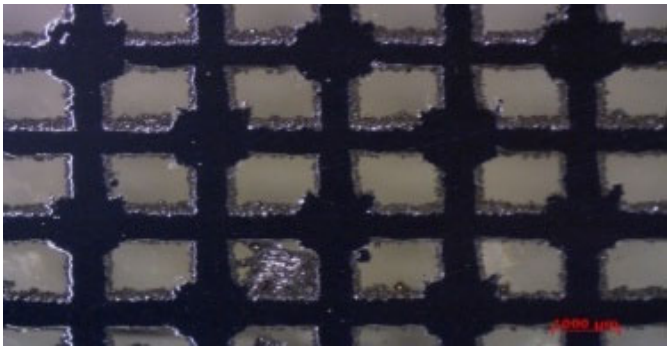

(a) Microscopy image at 25x magnification.

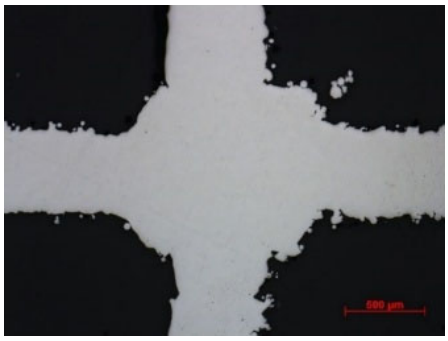

(b) Microscopy image at 50x magnification.

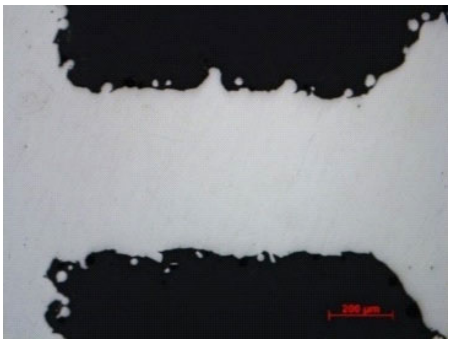

(c) Microscopy images at 100x magnification.

Figure 9. Standard microscopy images.

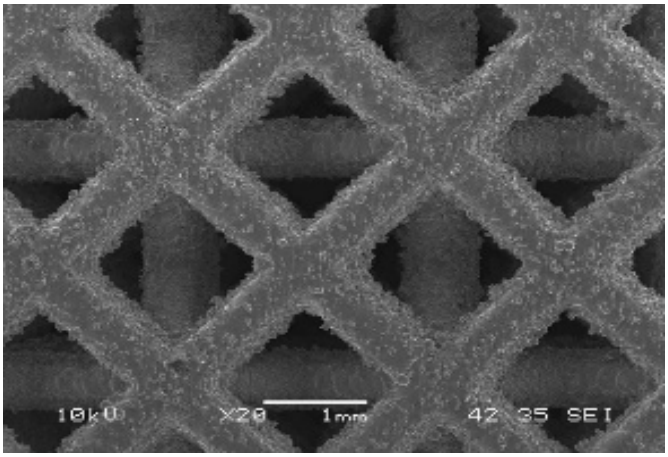

(a) Cubic scaffold.

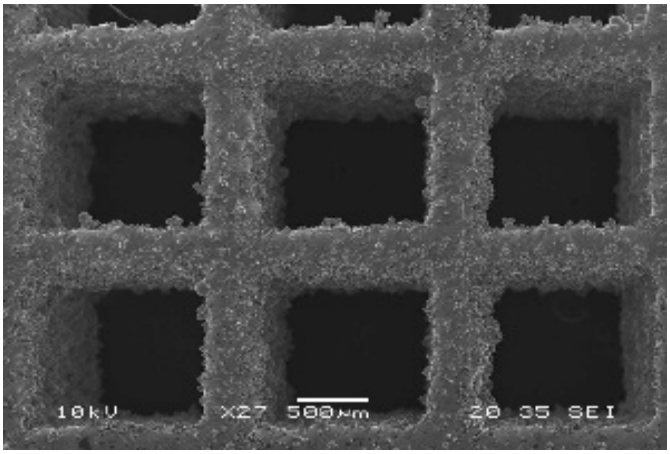

(b) Diagonal scaffold.

Figure 10. SEM images.

The dry weighing method was used to determine the relative structural density of the manufactured scaffolds. Weighing the samples was accomplished at normal room temperature and atmospheric conditions. The relative density of the cellular scaffolds was calculated by dividing the measured weight by the theoretical weight of the solid specimen. The theoretical weight was calculated using the theoretical density of the solid SS316L, as suggested by the manufacturer, which equaled 7.9 g/cm^3. Table 3 compares the relative structural density of the manufactured scaffold for each unit cell with the optimized scaffold designs. The average relative densities for cubic and diagonal scaffolds were 32.87% and 35.10%, respectively. The standard deviation for the cubic scaffold was 0.4105% and for the diagonal was 0.1602%. Comparing the manufactured scaffolds with optimized designs, the percentage error for the cubic and diagonal unit cells were 4.64% and 4.59%. Such results validate the consistency of the EOS M290 device in manufacturing BTE scaffolds using LPBF technology with high accuracy and precision.

Table 3. Comparison in relative structural densities between optimized design and manufactured scaffolds.

Unit Cell Design	Optimized Design (%)	Manufactured Scaffold (%)	Mean Manufactured	Std (%)
Cubic	34.47	32.97	32.87	0.41
		33.16		
		32.91		
		33.22		
		32.89		
		32.08		
Diagonal	36.79	35.09	35.10	0.16
		35.02		
		35.33		
		34.98		
		35.26		
		34.93		

Validating FEA Results by Experimental Testing

Stress-strain curves indicated typical foam behavior under compression, comprising elastic, plateau, and densification regions. Experimentally derived elastic moduli were 14.76 GPa (cubic) and 14.29 GPa (diagonal), closely aligning with FEA predictions. The failure analysis of Figure 11 shows that cubic scaffolds exhibited post-yield softening associated with stretch-dominated behavior, whereas diagonal scaffolds demonstrated bending-dominated failure suitable for energy absorption applications.

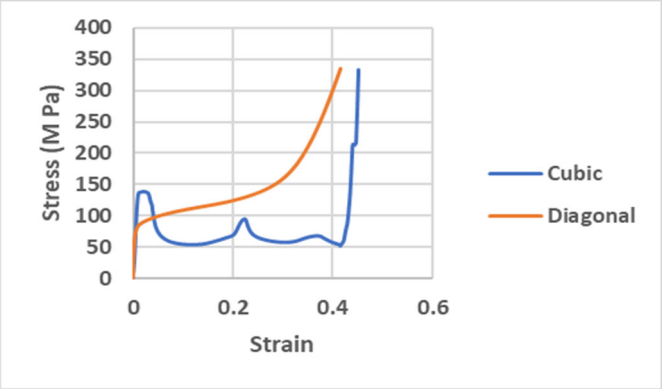

Figure 11. Experimental stress-strain curves for cubic and diagonal scaffolds.

The failure mechanisms for both designs agreed with the findings of Kadkhodapour et al. (2015). Uniform deformation of the vertical struts was observed in the cubic

scaffold. The stress fluctuations were related to the failure of the layer-by-layer mechanism due to the buckling of the struts. Once a layer was fully crushed, the second layer picked up the load and so on. The drop in stress after failure by plastic buckling is explained by the post-yield softening regime. Finally, the stress rose steeply at the densification strain when the post-yield ended for the final layer. Such behavior can be related to stretch-dominated structures, while for the diagonal scaffold, the entire structure was stressed once loading started.

Initially, the linear elastic behavior was caused by the bending of the struts followed by failure due to the yielding of the struts in each layer. The structure continued to collapse at nearly constant stress (plateau stress), up until the cells on the opposite sides were forced into contact, causing the stress to rise steeply at the densification strain. Such behavior is related to bending-dominated structures. The observed post-yield softening and high compressive strength of the cubic scaffold are hallmarks of stretch-dominated lattices in which struts primarily carry axial loads and confer high structural efficiency desirable in applications needing compressive load-bearing, such as metaphyseal or femoral segments (Mora Sierra, Reinoso, Paggi & Moreno, 2022). By contrast, the extended plateau stress and strong energy absorption of the diagonal scaffold reflected bending-dominated behavior, exhibiting progressive, ductile collapse that is valuable for applications demanding impact absorption or energy dissipation, such as interbody spinal fusion cages or bone-implant interface zones.

This behavior helps distribute stress more uniformly, mitigate peak stress levels, and reduce stress shielding effects, aligning with key goals in contemporary orthopedics (Karmiris-Obratański, Georgakopoulos-Soares, Cichocki, Lisiecka-Graça, Papazoglou & Labeas, 2025). The post-yield softening occurring in stretch-dominated scaffolds (cubic) makes them less effective in applications where energy absorption is required. However, they are appropriate for applications that require high load bearing, which can be explained by the fact that the cubic scaffold has higher failure stress than the diagonal scaffold. The long and flat plateaus in bending-dominated scaffolds (diagonal) makes them a better option for energy-absorption applications.

Bending, Shear, and Effects of Porosity

Despite all scaffolds having had the same structural modulus, their behavior varied in bending and torsion. The bending and shear modulus were calculated using the equations shown previously for bending and torsion. The bending modulus for the cubic and diagonal scaffolds were 10.29 GPa and 16.03 GPa, respectively. The shear modulus was 1.39 GPa for the cubic scaffold and 14.52 GPa for the diagonal scaffold. The cubic scaffold had lower bending stiffness than the diagonal scaffold and much lower torsional bending stiffness. This can be explained by the 45-degree -oriented struts in the diagonal scaffold carrying the shear and bending stresses. Experimental testing is needed to study the mechanical behavior of the scaffolds under bending and shear.

Moreover, the effect of porosity (1 – relative density) on the compressive, bending, and shear moduli of the scaffolds was numerically investigated. As expected, the mechanical properties increased with an increase in the relative density. The mechanical properties of the scaffolds were normalized to the solid properties of stainless steel. All data points were fitted using the power law, and relationships between the mechanical properties of the scaffold and the relative density were generated. Figure 12 shows that, for the elastic gradient, the exponent of the power-law was 1.12 for the cubic and 1.34 for the diagonal scaffold. Figures 12-14 confirm the findings that the stretch-dominated behavior for the cubic scaffold was stiffer and that the exponent was close to 1, which was lower than the exponent for the diagonal scaffold that exhibited bending-dominated failure.

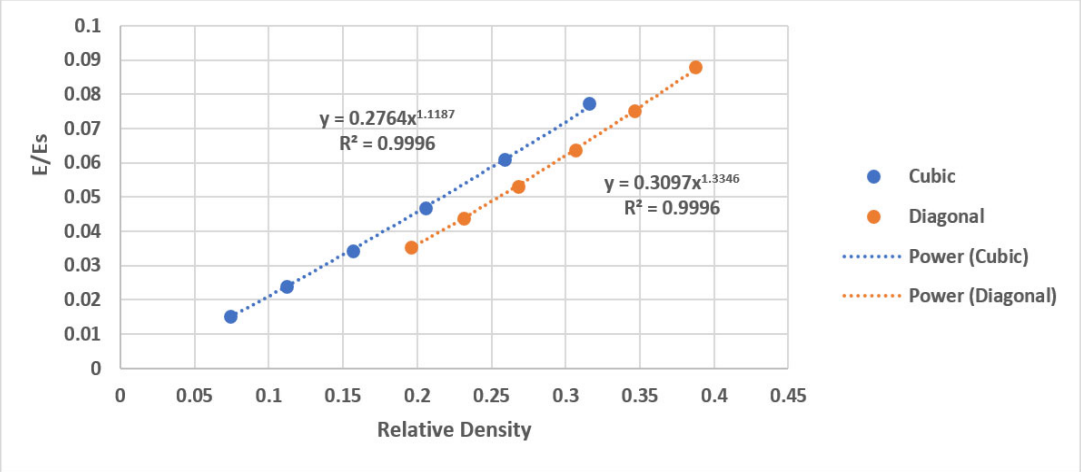

Figure 12. Effect of relative density on the structural modulus of the scaffold.

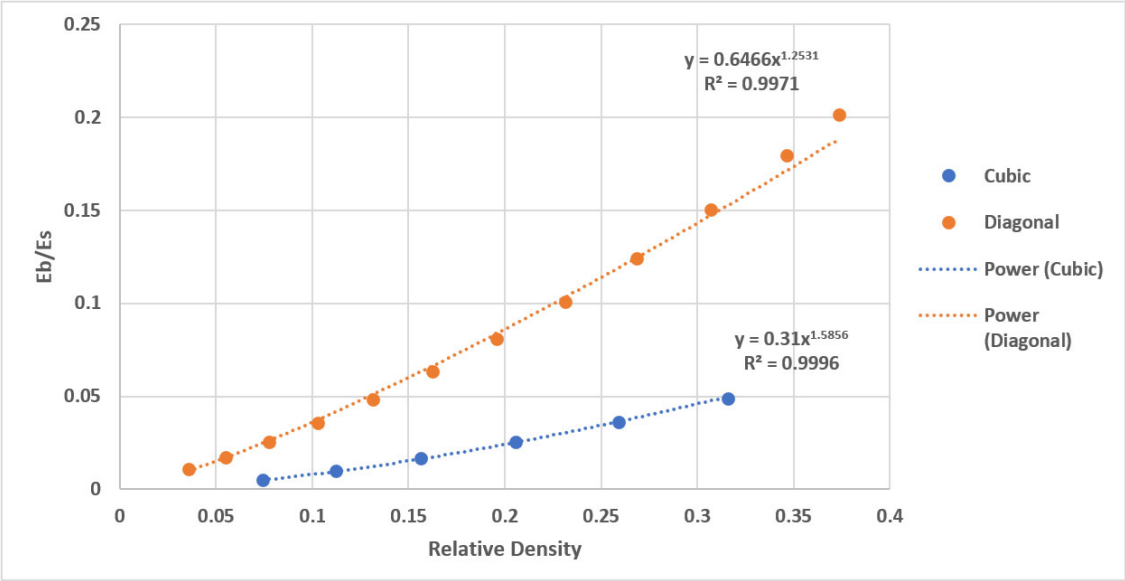

Figure 13. Effect of relative density on the bending modulus of the scaffold.

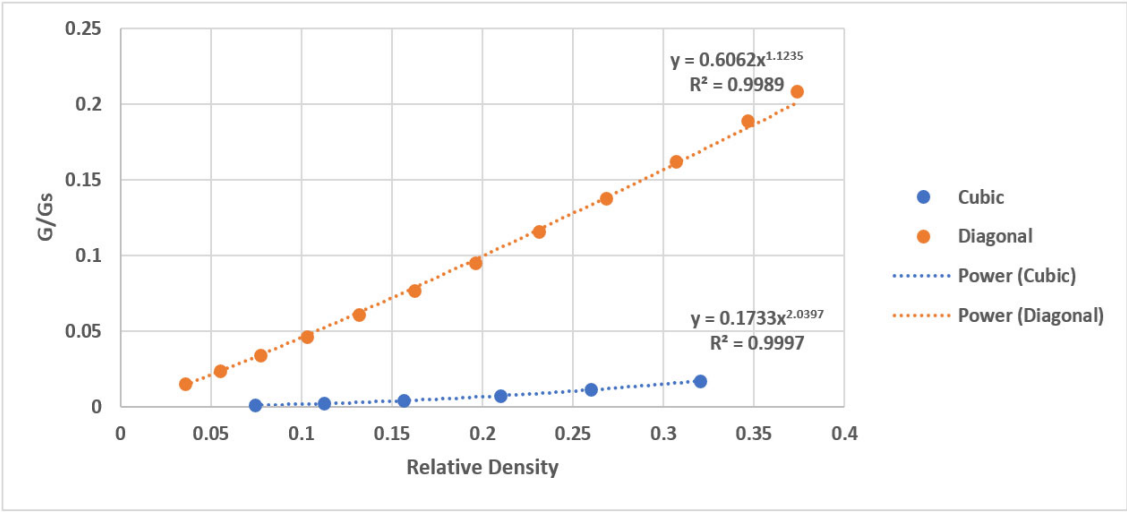

Figure 14. Effect of relative density on the shear modulus of the scaffold.

The exponents of the power-law for the bending stiffness of the cubic and diagonal scaffolds were 1.586 and 1.25, respectively, and the exponents of the power-law for the shear stiffness of the cubic and diagonal scaffolds were 1.12 and 2.04, respectively. The diagonal scaffold exhibited much higher bending and shear stiffnesses than the cubic scaffold. In addition, a slight increase in the bending and shear stiffnesses of the cubic scaffold was observed, while increasing the relative density of the cubic scaffold. However, the bending and shear moduli of the diagonal were considerably affected by the relative structural density of the scaffold. Comparison of the mechanical properties between the bone scaffolds and cortical bone.

Table 4 summarizes the relationships relating the elastic properties with the relative structural relative density of the scaffolds. Table 5 presents a comparison between the elastic stiffnesses of the cubic and diagonal scaffolds with the cortical bone properties are presented. The compressive modulus of both scaffolds fell in the elastic modulus range of cortical bone loaded longitudinally. The bending modulus of the diagonal scaffold fell in the cortical bone range loaded longitudinally, while the bending modulus of the cubic scaffold was slightly less than the cortical bone modulus. The shear modulus of the cubic scaffold was slightly lower than the cortical bone modulus, while the diagonal scaffold shear modulus was substantially higher than the shear modulus of the cortical bone.

Table 4. Relationships between the elastic properties of the scaffolds and their relative structural density.

	Cubic Scaffold	Diagonal Scaffold
Structural Modulus	$\frac{E^*}{E_s} = 0.276\left(\frac{\rho^*}{\rho_s}\right)^{1.12}$	$\frac{E^*}{E_s} = 0.310\left(\frac{\rho^*}{\rho_s}\right)^{1.34}$
Bending Modulus	$\frac{E_b^*}{E_{bs}} = 0.310\left(\frac{\rho^*}{\rho_s}\right)^{1.59}$	$\frac{E_b^*}{E_{bs}} = 0.6466\left(\frac{\rho^*}{\rho_s}\right)^{1.25}$
Shear Modulus	$\frac{G^*}{G_s} = 0.173\left(\frac{\rho^*}{\rho_s}\right)^{2.04}$	$\frac{G^*}{G_s} = 0.606\left(\frac{\rho^*}{\rho_s}\right)^{1.12}$

Table 6 presents a comparison of the values for compressive strength, flexural yield strength, ultimate flexural strength, and energy absorption of both scaffold designs with the cortical bone properties. The compressive strength of the cubic scaffold fell in the range of values of compressive strength for cortical bone loaded longitudinally. In comparison, the diagonal scaffold exhibited less compressive strength than the cortical bone loaded longitudinally. However, the diagonal scaffold compressive strength was observed to be comparable to the cortical bone loaded transversely. The flexural yield strength of both scaffold designs fell in the range of flexural strength values for cortical bone loaded longitudinally. The same was observed for the ultimate strength. As previously stated, the energy absorbed by the cubic scaffold was observed to be comparable to the cortical bone loaded transversely, while the energy absorbed by the diagonal scaffold was observed to be comparable to the cortical bone loaded longitudinally.

Conclusions

This study demonstrated the potential to generate customized, effective elastic moduli that match human cortical bone (~15 GPa) and thoroughly tested the mechanical and structural properties of scaffolds made of 316L stainless steel via additive manufacturing. A distinct structure-property relationship between unit-cell architecture and the deformation process was identified by the integrated computational-experimental approach, which combined finite element analysis with mechanical testing and microscopic characterization. The diagonal lattice design exhibited bending-dominated behavior, which demonstrated improved energy-absorption properties (33.55 MJ/m³) suitable for applications needing mechanical energy dissipation, such as cranial implants and fracture fixation systems.

These results support the possibility of using structurally customized SS316L scaffolds to create orthopedic implants tailored to each patient that solve the crucial problem of stress shielding via biomechanical compatibility. An important step in avoiding aseptic loosening and enhancing long-term therapeutic results is the shown capacity to concurrently match the strength and elastic modulus properties of natural bone while preserving the necessary porosity

Table 5. Comparison between the elastic stiffnesses of the cubic and diagonal scaffolds with the cortical bone properties.

	Cubic Scaffold	Diagonal Scaffold	Cortical Bone			
	FEA	Exp	FEA	Exp.	Longitudinal	Transverse
Comp. Modulus (GPa)	15.0	14.76	15.0	14.29	10-20	11.5
Bending Modulus (GPa)	10.29	9.49	16.03	14.76	12.8-19.3	4.7-7.9
Shear Modulus (GPa)	1.39	0.883	14.52	12.85	3.3-6.1	N/A

Table 6. Comparison of mechanical strength between bone scaffolds and cortical bone.

	Cubic Scaffold	Diagonal Scaffold	Cortical Bone	
			Longitudinal	Transverse
Comp. Strength (MPa)	138	75	90-175	24-62
Flexural Yield Strength (MPa)	107	113	100-131	43-63
Ultimate Flexural Strength (MPa)	148	195	121-152	43-71
Energy to Ultimate (MJ/m^3)	4.97	33.55	10.5-24.8	0.25-1.53

for biological integration. To move closer to clinical translation, a number of research directions should be explored further. These include investigating surface functionalization strategies to boost biological activity, developing multiscale modeling approaches that incorporate bone remodeling mechanisms, conducting thorough in vivo studies to assess osseointegration and long-term biocompatibility, and examining high-cycle fatigue behavior under physiological loading conditions. Validating the clinical applicability of these optimized scaffold designs and creating strong design recommendations for orthopedic solutions tailored to individual patients would require these investigations.

Acknowledgments

The authors would like to thank Mr. Ahmad Amer, UW-Milwaukee for help with editing, Prof. Ben Church UW-Milwaukee, and Prof. Dan Thoma, UW-Madison for providing experimental, laboratory logistics, and advisement in order to complete this research.

References

Abou-Ali, A. M., Al-Ketan, O., Rowshan, R., & Abu Al-Rub, R. (2019). Mechanical Response of 3D Printed Bending-Dominated Ligament-Based Triply Periodic Cellular Polymeric Solids. *Journal of Materials Engineering and Performance, 28*(6), 2316-2326. https://doi.org/10.1007/s11665-019-03982-8

Al-Ketan, O., Rowshan, R., & Abu Al-Rub, R. K. (2018). Topology-mechanical property relationship of 3D printed strut, skeletal, and sheet based periodic metallic cellular materials. *Additive Manufacturing, 19*, 167-183. https://doi.org/10.1016/j.addma.2017.12.006

Asadi-Eydivand, M., Solati-Hashjin, M., Fathi, A., Padashi, M., & Abu Osman, N. A. (2016). Optimal design of a 3D-printed scaffold using intelligent evolutionary algorithms. *Applied Soft Computing, 39*, 36-47. https://doi.org/10.1016/j.asoc.2015.11.011

DebRoy, T., Wei, H. L., Zuback, J. S., Mukherjee, T., Elmer, J. W., Milewski, J. O. ...Zhang, W. (2018). Additive manufacturing of metallic components – Process, structure and properties. *Progress in Materials Science, 92,* 112-224. https://doi.org/10.1016/j.pmatsci.2017.10.001

Jukes, J. M., Both, S. K,. Leusink, A., Sterk, L. M., Th., van Blitterswijk, C. A., & de Boer, J. (2008). Endochondral bone tissue engineering using embryonic stem cells. *Applied Biological Sciences, 105*(19), 6840-6845. https://doi.org/10.1073/pnas.0711662105

Kadkhodapour, J., Montazerian, H., Darabi, A. Ch., Anaraki, A. P., Ahmadi, S. M., Zadpoor, A. A., & Schmauder, S. (2015). Failure mechanisms of additively manufactured porous biomaterials: Effects of porosity and type of unit cell. *Journal of the Mechanical Behavior of Biomedical Materials, 50*, 180-191. https://doi.org/10.1016/j.jmbbm.2015.06.012

Karageorgiou, V., & Kaplan, D. (2005). Porosity of 3D biomaterial scaffolds and osteogenesis. *Biomaterials, 26* (27), 5474-5491. https://doi.org/10.1016/j.biomaterials.2005.02.002

Karmiris-Obratański, P., Georgakopoulos-Soares, I., Cichocki, K., Lisiecka-Graça, P., Papazoglou, E. L., & Labeas, G. N. (2025). Compressive and energy absorption properties of titanium hybrid lattice structures for bioimplant applications fabricated via LPBF. *Materials & Design, 254,* 114045. https://doi.org/10.1016/j.matdes.2025.114045

Kurzynowski, T., Gruber, K., Stopyra, W., Kuźnicka, B., & Chlebus, E. (2018). Correlation between process parameters, microstructure and properties of 316 L stainless steel processed by selective laser melting. *Materials Science and Engineering: A, 718*, 64-73. https://doi.org/10.1016/j.msea.2018.01.103

Leuders, S., Thöne, M., Riemer, A., Niendorf, T., Tröster, T., Richard, H. A., & Maier, H. J. (2013). On the mechanical behaviour of titanium alloy TiAl6V4 manufactured by selective laser melting: Fatigue resistance and crack growth performance. *International Journal of Fatigue, 48,* 300-307. https://doi.org/10.1016/j.ijfatigue.2012.11.011

Lewandowski, J. J., & Seifi, M. (2016). Metal Additive Manufacturing: A Review of Mechanical Properties. *Annual Review of Materials Research, 46*, 151-186. https://doi.org/10.1146/annurev-matsci-070115-032024

Li, J. P., Habibovic, P., van den Doel, M., Wilson, C. E., de Wijn, J. R., van Blitterswijk, C. A., & de Groot, K. (2007). Bone ingrowth in porous titanium implants produced by 3D fiber deposition. *Biomaterials 28*, 2810 -2820.

Lin, C. Y., Kikuchi, N., & Hollister, S. J. (2004). A novel method for biomaterial scaffold internal architecture design to match bone elastic properties with desired porosity. *Journal of Biomechanics, 37*, 623-636. https://doi.org/10.1016/j.jbiomech.2003.09.029

Ma, X., Zhang, D. Z., Zhao, M., Jiang, J., Luo, F., & Zhou, H. (2022). Mechanical and energy absorption properties of functionally graded lattice structures based on minimal curved surfaces. *The International Journal of Advanced Manufacturing Technology, 118*, 995-1008. https://doi.org/10.1007/s00170-021-07768-y

Maskery, I., Aboulkhair, N. T., Aremu, A. O., Tuck, C., Ashcroft, I., Wildman, R., & Hague, R. J. M. (2016). A mechanical property evaluation of graded density Al-Si10-Mg lattice structures manufactured by selective laser melting. *Materials Science and Engineering: A, 670*, 264-274. https://doi.org/10.1016/j.msea.2016.06.013

Masuo, H., Tanaka, Y., Morokoshi, S., Yagura, H., Uchida, T., Yamamoto, Y., & Murakami, Y. (2018). Influence of defects, surface roughness and HIP on the fatigue strength of Ti-6Al-4V manufactured by additive manufacturing. *International Journal of Fatigue, 117,* 163-179. https://doi.org/10.1016/j.ijfatigue.2018.07.020

Mora Sierra, D. C., Reinoso, J., Paggi, M., & Moreno, R. (2022). Numerical investigation of Ti6Al4V gradient lattice structures with tailored mechanical response. *Advanced Engineering Materials, 24*(4), 2101760. https://doi.org/10.1002/adem.202101760

Murr, L. E., Gaytan, S. M., Medina, F., Lopez, H., Martinez, E., Machado, B. I. ...Bracke, J. (2010). Next-generation biomedical implants using additive manufacturing of complex cellular and functional mesh arrays. *Philosophical Transactions of the Royal Society A: Mathematical, Physical and Engineering Sciences, 368* (1917), 1999-2032. https://doi.org/10.1098/rsta.2010.0010

Novich, A. N., Sánchez, J. A., Paniagua, J. M., & Mantell, S. C. (2024). *Experimental examination of additively manufactured SS316L and Al6061: Accuracy of DIC strain measurements*. Experimental Mechanics. Springer. https://doi.org/10.1007/s11340-024-01076-8

Öhman, C., Baleani, M., Pani, C., Taddei, F., Alberghini, M., Viceconti, M., & Manfrini, M. (2011). Compressive behaviors of children and adult cortical bone. *Bone, 49*, 769-776. https://doi.org/10.1016/j.bone.2011.06.035

Ponader, S., von Wilmowsky, C., Widenmayer, M., Lutz, R., Heinl, P., Körner, C. ...Schlegel, K. A. (2010). In vivo performance of selective electron beam-melted Ti-6Al-4V structures. *Journal of Biomedical Materials Research, 92A*(1), 56-62. https://doi.org/10.1002/jbm.a.32337

Rankouhi, B., Bertsch, K. M., Meric de Bellefon, G., Thevamaran, M., Thoma, D. J., & Suresh, K. (2020). Experimental validation and microstructure characterization of topology optimized, additively manufactured SS316L components. *Materials Science and Engineering: A, 776*, 139050. https://doi.org/10.1016/j.msea.2020.139050

Rodgers, G. W., Van Houten, E. E. W., Bianco, R. J., Besset, R., & Woodfield, T. B. F. (2014). Topology Optimization of Porous Lattice Structures for Orthopaedic Implants. *Proceedings of the International Federation of Automatic Control*, 47(3), 9907-9912. https://doi.org/10.3182/20140824-6-ZA-1003.00924

Taniguchi, N., Fujibayashi, S., Takemoto, M., Sasaki, K., Otsuki, B., Nakamura, T. …Matsuda, S. (2016). Effect of pore size on bone ingrowth into porous titanium implants fabricated by additive manufacturing: An in vivo experiment. *Materials Science and Engineering: C, 59,* 690-701. https://doi.org/10.1016/j.msec.2015.10.069

Wang, C., Xu, D., Li, S., Yi, C., Zhang, X., He, Y., & Yu, D. (2020). Effect of pore size on the physicochemical properties and osteogenesis of Ti-6Al-4V porous scaffolds with bionic structure. *ACS Omega, 5*(44), 28684-28692. https://doi.org/10.1021/acsomega.0c0382 4

Zhu, Y., Li, D., Wang, Y., Li, S. J., Hou, W. T., Hao, Y. L., Yang, R., & Misra, R. D. K. (2019). Additively manufactured metallic auxetic metamaterials for biomedical implants. *Acta Biomaterialia, 84,* 437–449. https://doi.org/10.1016/j.actbio.2018.12.046

Author Biographies

MOHAMMAD O. AL-BARQAWI is a structural engineer with CHA Consulting. Dr. Al-Barqawi may be reached at mbarqawi@chasolution.com

MUSTAFA MAHAMID is a research associate professor at the University of Illinois-Chicago. Dr. Mahamid may be reached at mmahamid@uic.edu

ADEEB RAHMAN is an associate professor in the Department of Civil and Environmental Engineering at the University of Wisconsin-Milwaukee. Dr. Rahman may be reached at adeeb@uwm.edu

Evaluating the Label Read Rate Using DOE–750 Labels

Rajesh Balasubramanian, University of Memphis; Kevin Berisso, University of Memphis

Abstract

During a radio frequency identification (RFID) study conducted at the AIDC Lab using a combination of different label counts, label inlays (NXP UCode 8 & NXP UCode 9) and label readers (CSL CS463, Impinj R700 and Zebra FX9600) at a fixed distance (7ft), the authors found that the 750-count labels had a disproportionate drop in unique reads (50%) for all time durations—3 seconds, 5 seconds, and 10 seconds. The number of labels used for the study were: 1, 10, 50, 100, 250, 500, 750, 1000, and 1500. Because numerous additional testing parameters (between 10 and 20 various RFID reader settings, as well as additional label classes) were desired, a reduction in the overall number of tests was necessary. The aim of the study was the use of the statistical design-of-experiments (DOE) approach for maximizing unique read rate by optimizing the ideal set of parameters for the 750-label count. This number of labels (750) is close to the median in the label count set and seems to emulate the most common label count used in industry for RFID operations.

Introduction

During an earlier study (Berisso & Balasubramanian, 2025), RAIN RFID was subjected to noise to simulate its effects on the unique readability of labels of different counts—1, 10, 50,100, 250, 500, 750, and 1500. Both NXP UCode 8 and NXP UCode 9, with both single and double-pitch separation, were deployed for that study. The authors noticed a definite deviation across all the label reads. The 750-label count stood out in all the tests, with noise and without, and was used as the basis of this current study. Nowadays, researchers primarily select the DOE based on the assumed importance of the factors and the desired number of experimental runs (Jankovic, Chaudhary & Goia, 2021). The DOE is a statistical methodology that is widely used in industry for such analyses. Where there are various inputs that can be both variable and binary, but there is a need to establish an optimized solution, DOE is highly effective (Allen, 2020). Figure 1 shows an example of a DOE setup and associated input factors that was employed to optimize an injection molding machine.

If the injection mold were to be tried by varying one factor at a time, the number of combinations would be 48 billion! On the other hand, if a DOE were deployed, the same could be accomplished with fewer than 50 combinations while still achieving the desired results. Thus, DOE is a very cost- and time-efficient tool used in industry (Paul, 2020).

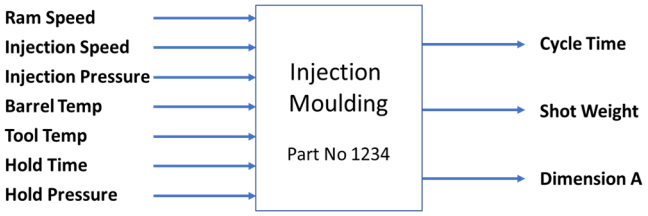

Ram Speed	**10 – 20**	**(10 Settings)**
Injection Speed	**40 – 60**	**(20 Settings)**
Injection Pressure	**100 – 150**	**(50 Settings)**
Barrel Temperature	**220 – 260**	**(40 Settings)**
Tool Temperature	**180 – 220**	**(40 Settings)**
Hold Time	**30 – 60**	**(30 Settings)**
Hold Pressure	**500 – 600**	**(100 Settings)**

Figure 1. An example of a DOE setup.

Background

Readability is an important key performance indicator (KPI) for the RFID industry. Accuracy combined with efficiency is the key to implementing robust label-reading solutions. The sooner the labels can be read is as important as all the labels being read correctly. For this DOE, the established times were 3 seconds, 5 seconds, and 10 seconds, with 3 seconds being optimistic, 10 seconds being the maximum time, and 5 seconds being ideal. Figure 2 shows the results from the RAIN RFID study by Berisso and Balasubramanian (2025). The read rates are expressed as a percentage. The term design of experiments, also known as experimental design, was coined by Ronald Fisher in the 1920s for his agricultural experiments. (Design of Experiments, n.d.) There are four eras of DOE: Agricultural origins, 1918-1920; Industrial, 1951-1970; Industrial Quality, 1970-1990; and, Modern, 1990-later. During the industrial quality era, quality improvement initiatives in many companies became management goals. Taguchi (Schmidt & Launsby, 1994) used DOE for robust parameter design and process robustness. The modern era has seen many industries deploy DOE, where economic competitiveness and globalization are driving all sectors of the economy to be more competitive (A Quick History of the Design of Experiments, n.d.).

DOE is defined as a branch of applied statistics that deals with planning, conducting, analyzing, and interpreting controlled tests to evaluate the factors that control the value of a parameter or group of parameters. DOE is a powerful data collection and analysis tool that can be used in a variety of experimental situations. It allows for multiple input factors to be manipulated to determine their effect on a desired output (response). By manipulating multiple inputs

simultaneously, DOE can identify important interactions that may be missed when experimenting with one factor at a time. All combinations can be investigated (full factorial) or only a portion of the possible combinations (fractional factorial). A strategically planned and executed experiment can provide a great deal of information about the effect on a response variable due to one or more factors. Many experiments involve holding certain factors constant while altering the levels of another variable. This "one factor at a time" (OFAT) approach to process knowledge is, however, inefficient when compared with simultaneously changing factor levels (Design of Experiments, n.d.). In the field of smart manufacturing, the use of automated machinery and analysis systems not only greatly improved production efficiency but also safety and stability (Hsu, Wang, Chen, Tsai & Lo, 2025).

RAIN RFID is the marketing name for ultra-high frequency radio frequency identification (RFID) solutions, the same as Wi-Fi is the marketing name for the ISO/IEEE 802.11 b/g/n technology that most people use for their wireless computer communications. RAIN RFID has been adopted by vast portions of the supply chain, including companies such as Wal-Mart, Macys, and even the U.S. Department of Defense (Delen, Hardgrave & Sharda, 2007) with over 52 billion tags shipped globally in 2024. Able to be read at distances of up to 50 feet, the technology uses energy harvesting to power the tags, resulting in a battery-less solution that is often referred to as passive RFID. Used extensively in some retail stores, such as Wal-Mart and Macy's, the tags allow for the unique identification of objects and increased efficiencies in inventory counting and tracking (Patton, Periaswamy, Dunn & McDaniel, 2023).

Methodology

The lab used in this current study had limited time availability. The lab was used for many other industrial studies, so there was a time constraint. The method adopted to conduct an effective DOE was based on continued brainstorming discussions. A process of elimination was adopted to ensure that the DOE was executed with a definite goal and approach. The other factors considered were to keep the experiment at a higher level with the understanding that, if needed, the study could go one level deeper. Higher level implies that the factors themselves have min/max settings and not settings at a lower level that could be adjusted to get that extra desired output. The primary objective of this DOE was to study and see if the higher-level factors were indeed the prime factors that contributed to the read rate. If so, then were they independently contributing, or was there an interaction between them that contributed to the output? The standard DOE methodology is comprised of two steps. Although it is impractical to replicate all possible conditions present in systems, the chosen parameters and their ranges offered a realistic and representative simplification under investigation (Trotta, Binda, Ferrario, Pozzi & Michetti, 2026).

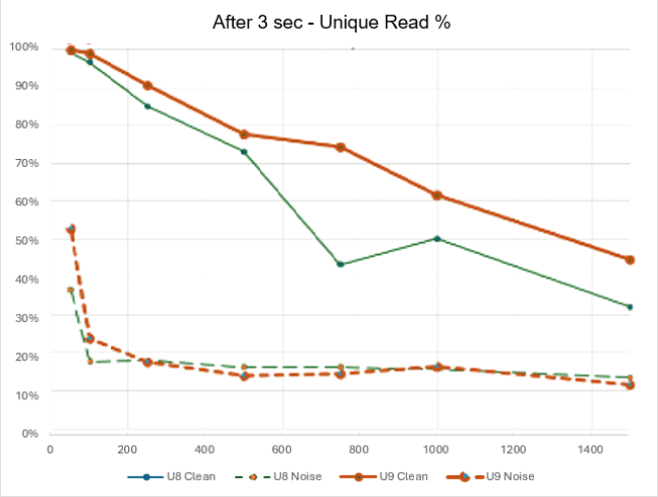

(a) Read rate for 3 seconds.

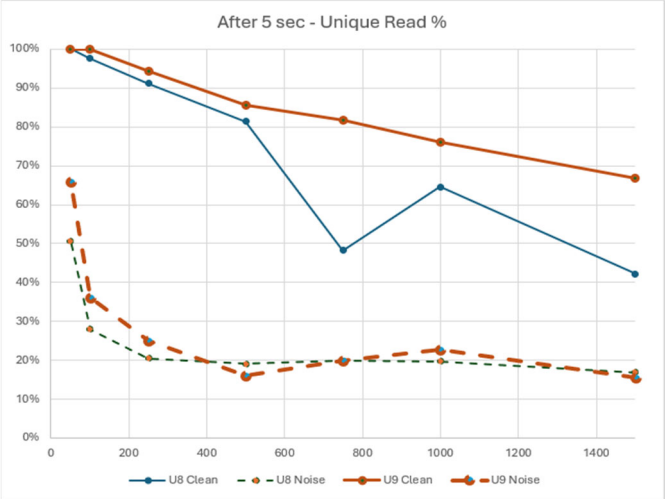

(b) Read rate for 5 seconds.

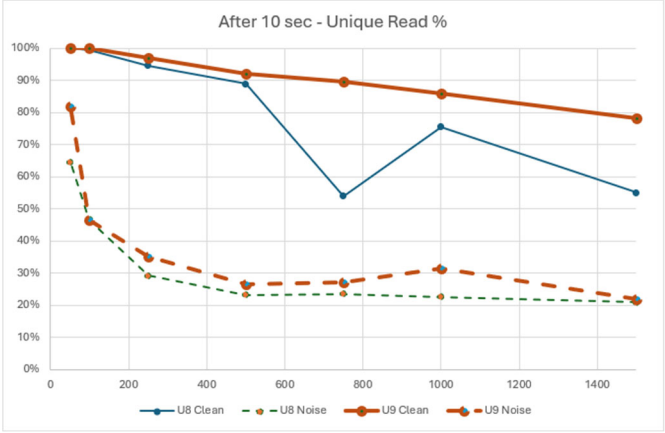

(c) Read rate for 10 seconds.

Figure 2. Established read times for the DOE.

Screening is typically the first step, where all potential contributing input factors are screened and ranked. Also known as the Taguchi screening, it is particularly useful when beginning with multiple unknowns. In this current case, the experiment was limited; mostly it was a survey or input from subject matter experts that was used. Modeling was the second step, where the key independent factors from the screening outputs are finalized as the key contributing factors. The factors are set up in a structured manner known as an orthogonal array. This is especially important because any error in the setup of the experiment will invalidate all results. Orthogonal experimental design is an efficient experimental design method based on orthogonal arrays, the aim of which is to systematically study the effects of multiple factors and their levels on experimental outcomes with a limited number of trials (Li et al., 2025).

The DOE consultant, Paul Allen, provided valuable information to ensure there were no errors. The consultant provided solutions to industry using DOE methodology. The consultant did not have any idea about the setup but consulted only about the theoretical aspects of the experiment. There was no screening done for this DOE because the key factors were identified during the initial RAIN RFID study. However, there were still many factors from that study that were revisited to make the experiment as effective as possible. The initial factors that were listed were

- Distance of the antenna to the label board
- Label family: Zebra UCode8 or NXP UCode9
- Label pitch: single or double
- Reader setup: Session 0 or Session 1
- Readers: Zebra, Impinj, or any other
- Should noise inducers be used?
- Number of antennas – 1 or 2
- Other software setups

After a brainstorming session and with input from the DOE consultant, the input factors were shortened to the following.

- Distance of the antenna to the label board
- Label family: Zebra UCode8 or NXP UCode9
- Label pitch: single or double
- Reader setup: Session 0 or Session 1

It was also decided that the experiment would be split by readers—only Zebra and Impinj—and be conducted independently as a separate DOE. Zebra and Impinj are very prominent RFID readers extensively used in industry worldwide. The models are mostly widely used as well. Sigma XL, which is an add-in to *Excel*, was used to set up the experiment, gather data, and perform analyses. Table 1a shows the original values. The software accepts only coded values for setup and processing. Table 1b shows the coded values. Tables 2a-b show the factors, the orthogonal array, and the setup sheet for readers.

Table 1a. Original and coded values for software input.

Uncoded		
Reader Session	S0	S1
Label Family	U8	U9
Distance from Reader (feet)	6	8
Label Pitch	Single	Double

Table 1b. Coded values for software input.

Coded		
Reader Session	-1	1
Label Family	-1	1
Distance from Reader (feet)	-1	1
Label Pitch	-1	1

The RFID tags used for the test were Avery Dennison Belt tags with the NXP UCode 8 and NXP UCode 9 chips. The NXP UCode 8 tag is an older generation tag relative to the UCode 9 tag, with the primary difference being that the UCode 9 is slightly more sensitive. The other primary differences (write speeds, memory size, etc.) were not assumed to have had an impact on this study. The RAIN RFID tags were combined with a 73mm x 17mm label and were encoded with unique values in the EPC memory so that each tag was uniquely identifiable, both within and between groups. Because of the default pitch of the UCode 8 tags as they came from Avery Dennison, the labels were placed on heavy printer paper to make the mounting and moving of the tags as similar as possible between the two sets.
The equipment used for the tests was as follows:

- Impinj R700 four-port reader – RFID reader
- Zebra FX9600 eight-port reader – RFID reader
- Two eight dBi circular polarized antennas (attached to RFID readers)

The test was conducted inside the AutoID lab at the University of Memphis. Care was taken to ensure that all metal objects were removed behind the antennas to avoid any type of error or interference. The area around the test board was cleared of all existing tags. While initial tests showed that no tags were within range, up to ten tags did occasionally show up in the recorded data, indicating that the space was not as empty as originally believed. However, continued attempts to find the wayward tags failed to locate them, so it was determined that they would just be purged from the dataset during post-processing. Figures 3a and 3c show the test environment, while Figure 3b shows the distance layout, which was marked on the floor. The label sets were prepared ahead of time, and the flow of testing was designed in such a way that minimal changes were needed to avoid any setup errors. After label swaps, care was taken to ensure that labels were placed in quarantined areas to avoid any signal inference or false readings. All readers ran for 20 seconds, and there were three iterations recorded for each setup, as per the design requirements.

Table 2a. The test setup, including the factors studied for the Zebra reader.

Zebra FX9600							
Row#	Label Pitch	Label Family	Distance	Reader Session	Output 1	Output 2	Output 3
1	-1	-1	-1	-1			
2	-1	-1	-1	-1			
3	-1	-1	1	1			
4	-1	-1	1	1			
5	-1	1	-1	-1			
6	-1	1	-1	-1			
7	-1	1	1	1			
8	-1	1	1	1			
9	1	-1	-1	-1			
10	1	-1	-1	-1			
11	1	-1	1	1			
12	1	-1	1	1			
13	1	1	-1	-1			
14	1	1	-1	-1			
15	1	1	1	1			
16	1	1	1	1			

Table 2b. The test setup, including the factors studied for the Impinj reader.

Impinj R700							
Row#	Label Pitch	Label Family	Distance	Reader Session	Output 1	Output 2	Output 3
1	-1	-1	-1	-1			
2	-1	-1	-1	-1			
3	-1	-1	1	1			
4	-1	-1	1	1			
5	-1	1	-1	-1			
6	-1	1	-1	-1			
7	-1	1	1	1			
8	-1	1	1	1			
9	1	-1	-1	-1			
10	1	-1	-1	-1			
11	1	-1	1	1			
12	1	-1	1	1			
13	1	1	-1	-1			
14	1	1	-1	-1			
15	1	1	1	1			
16	1	1	1	1			

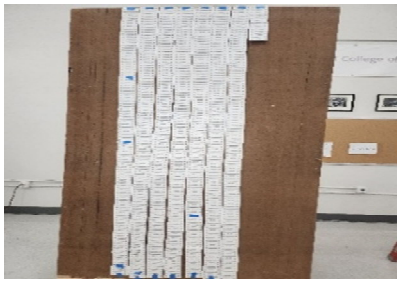

(a)
A picture of the label arrangement for the experiment.

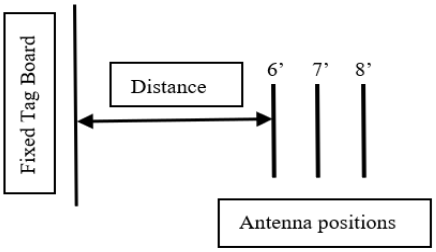

(b)
The distances between the readers and the label board.

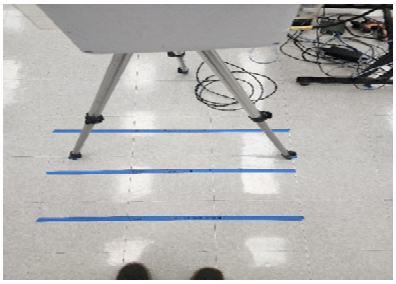

(c)
Markings on the floor indicating distance.

Figure 3. The test environment.

Table 3a. Zebra regression analysis output before rerun.

Zebra FX9600							
		3 Seconds		5 Seconds		10 Seconds	
Factor	Name	Coeff	P(2Tail)	Coeff	P(2Tail)	Coeff	P(2Tail)
A	Label Pitch	10.23	0.000	8.38	0.000	6.66	0.000
B	Label Family	12.74	0.000	11.40	0.000	10.26	0.000
C	Distance	-3.59	0.005	-2.42	0.020	-1.78	0.027
D	Reader Session	2.52	0.0111	1.98	0.055	1.494	0.062
AB			0.007	-7.30	0.000	-6.51	0.000
AC			0.029				
BC			0.077				

Table 3b. Impinj regression analysis output before rerun.

Impinj R700							
		3 Seconds		5 Seconds		10 Seconds	
Factor	Name	Coeff	P(2Tail)	Coeff	P(2Tail)	Coeff	P(2Tail)
A	Label Pitch	0.90	0.000	1.08	0.000	1.41	0.000
B	Label Family	15.63	0.000	10.85	0.000	7.21	0.000
C	Distance	1.95	0.000	0.75	0.000	0.14	0.000
D	Reader Session	1.99	0.000	0.77	0.055	0.156	0.000
AB		-1.50	0.000	-2.81	0.000	-2.51	0.000
AC		1.95	0.000	0.69		0.15	
AD		1.92	0.000	0.68		0.14	

In total, 96 individual files were generated, which were later compiled into three worksheets for 3 seconds, 5 seconds, and 10 seconds before further processing for analysis. After the data were obtained, a regression analysis was the next step. In the initial analysis, some of the interactions with p-values less than 0.05 were removed and the analysis was rerun. P values greater than 0.05 indicate that the factors are not significant to the read rate. Tables 3a-b show how the software highlighted significant interactions in red or blue. After rerunning the regression analysis, the software was used to optimize the results. These were the settings that were included in the results.

Output

Separate analyses were conducted using Zebra and Impinj readers to allow for a comparison between the two. Because these readers operated on different setups, it was necessary to keep them separated. The read times for the read rate remained at 3 seconds, 5 seconds, and 10 seconds. For each reading time, the software produced two plots: Y-Hat and S-Hat, also known as the marginal means plots in DOE. The Y-Hat chart is the most important for this study, as the goal was to improve the read rate. These outputs demonstrated the effect of each factor on the read rate independently, as well as any interactions that may have influenced the results. The X-axis displays the input factors, while the Y-axis shows the read rate. Figure 4 shows the three outputs plots for the Zebra reader—the Y Hat plots for 3 seconds, 5 seconds, and 10 seconds. For the Impinj reader, the results were different. Figure 5 shows the three outputs for the Impinj reader—the Y Hat plots for 3 seconds, 5 seconds, and 10 seconds. The results for the Zebra reader showed no interactions between the factors, but there was variation when the settings were changed from low to high. Based on the regression analysis, the results were optimized to achieve a 100% read rate.

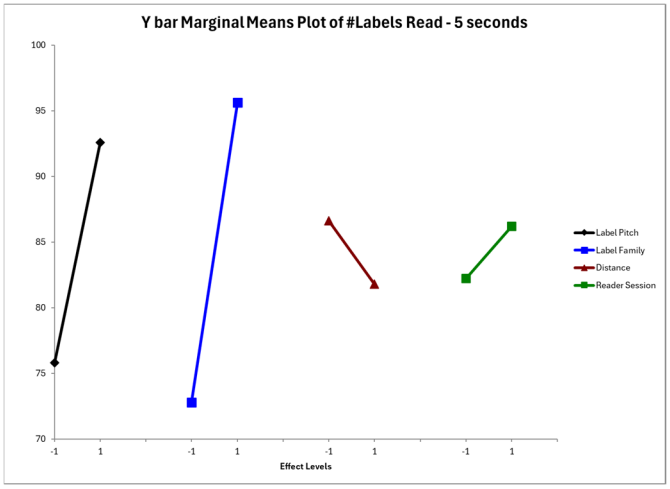

(a) Y bar marginal means plot (3 seconds).

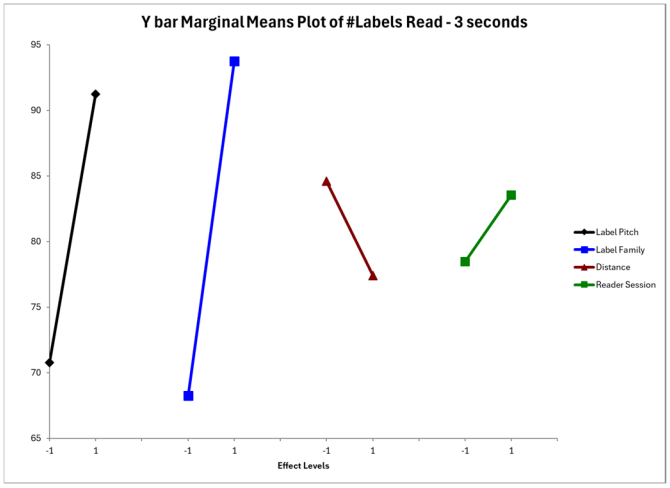

(b) Y bar marginal means plot (5 seconds).

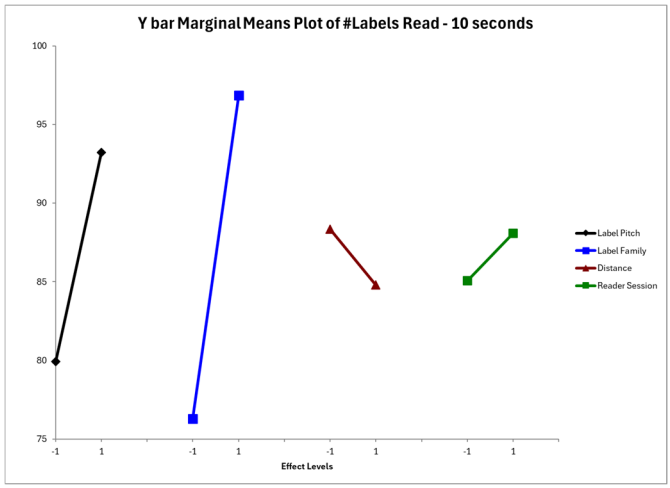

(c) Y bar marginal means plot (10 seconds).

Figure 4. Y Hat plots for the Zebra readers.

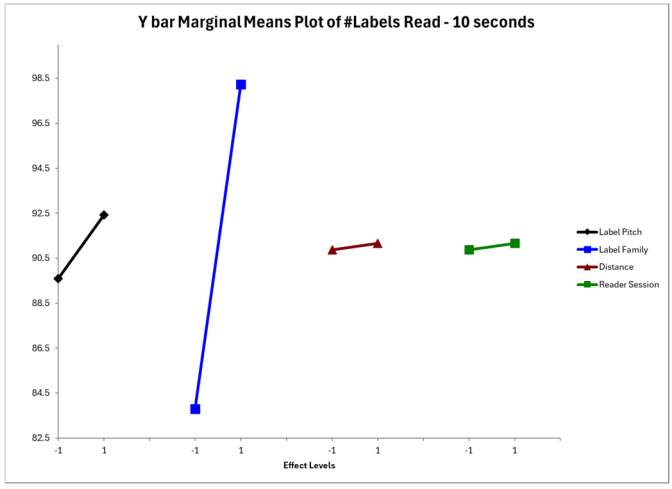

(a) Y bar marginal means plot (3 seconds).

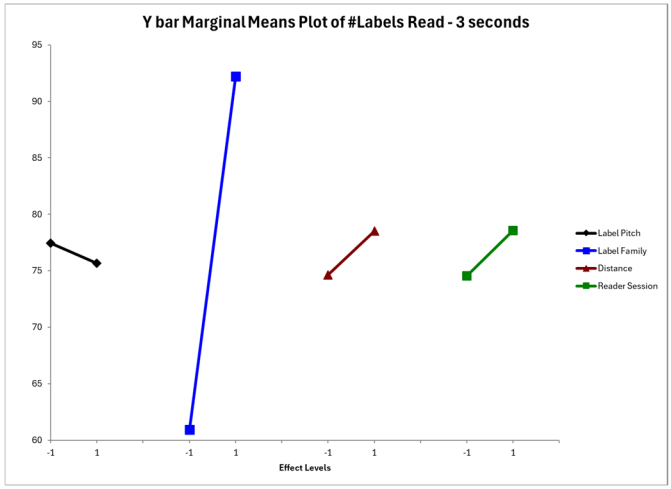

(b) Y bar marginal means plot (5 seconds).

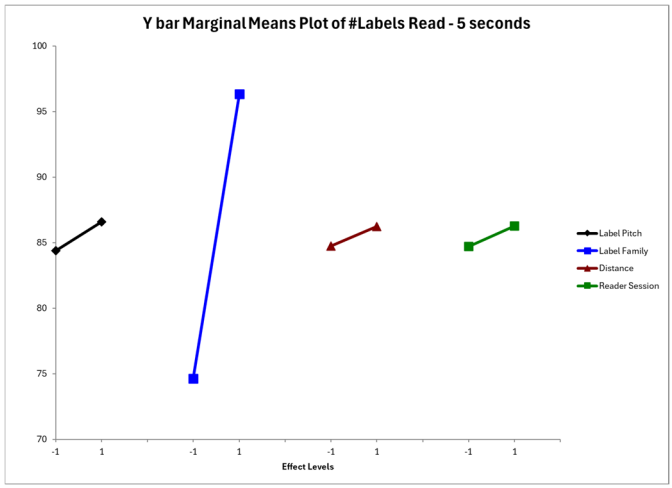

(c) Y bar marginal means plot (10 seconds).

Figure 5. Y Hat plots for the Impinj readers.

Table 4 shows the output of the software. The results for the Impinj reader showed no interactions between the factors, but there was variation when the settings were changed from low to high. As a next step, a regression analysis was done and the results were optimized with the objective of attaining a read rate of 100%. Table 5 shows the output of the software.

Table 4. Optimized settings for Zebra FX9600.

Factor	Name	Low	High	Value
A	Label Pitch	-1	1	1
B	Label Family	-1	1	1
C	Distance	-1	1	0.687
D	Reader Session	-1	1	1

Table 5. Factors and optimized settings for Impinj R700.

Factor	Name	Low	High	Value
A	Label Pitch	-1	1	0.450
B	Label Family	-1	1	1
C	Distance	-1	1	1
D	Reader Session	-1	1	1

Results

The results of the Impinj experiment suggested that, for the best read rate, the label pitch had to be half pitch (i.e., 50% of the single pitch). However, the NXP UCode 9 labels were ideal with a 6-foot distance from the reader, while reader session 1 was the best. This Zebra experiment suggested that, for the best read rate, the single label pitch was ideal, NXP UCode 9 labels were ideal, the ideal distance of the reader (~7.7') would be optimum, and reader session 1 was the best. Setting up the DOE independently for both readers proved to be a good decision, as suggested by the consultant. The common factors were the label family and the reader sessions. The differences in label pitch and distance could be further analyzed as separate DOE, if needed for future experimentation. Using the DOE methodology provided a greater insight into factor analysis. The read-rate variations between Impinj and Zebra suggested that each had different capabilities by design, and adjusting sub-parameters would be necessary to improve their output. Further study is needed in this area.

Acknowledgements

The authors would like to thank Mr. Paul Allen for his support in understanding the study and providing guidance during the setup phase. The authors express their gratitude to him for his offer of support during the result analysis and consultation with the conclusions drawn and further advice. RAIN RFID tags were provided thanks to Mr. Jason Ivy, Logistics Solution Consultant Director for Avery Dennison, and Mr. Louis Parker, IoT/RFID Market Manager – Logistics, Packaging & Supply Chain of Checkpoint Systems – a CCL Industries company. The Impinj R700 reader was donated thanks to Dr. Megan Brewster, VP Advanced Technology at Impinj, and the Zebra FX9600 reader was donated to the AutoID Lab by Mr. Michael Fein and Mr. Anthony Tortorello of Zebra.

References

A Quick History of the Design of Experiments (DOE) (n.d.). https://online.stat.psu.edu/stat503/book/export/html/633

Berisso, K., & Balasubramanian, R (2025). Potential Impacts of NextNav on RAIN RFID. *International Journal of Engineering Research & Innovation, 17*(1), 5-10. https://ijeri.org/IJERI-Archives/issues/spring2025/X__IJERI%20spring%202025%20v17%20n1.pdf

Delen, D., Hardgrave, B. C., & Sharda, R. (2007). RFID for better supply-chain management through enhanced information visibility. *Production and operations management*, *16*(5), 613-624. https://doi.org/10.1111/j.1937-5956.2007.tb00284.x

Design of Experiments (n.d.). https://safetyculture.com/topics/design-of-experiments/

Hsu, T-Y., Wang, C-C., Chen, Y-W., Tsai, C-H., & Lo, C-Y. (2025). Dielectric design for sensitivity maximization in force sensors through full-factorial experiment method and desirability function. *Measurement 256*, 118252. https://www.sciencedirect.com/science/article/abs/pii/S0263224125016112

Jankovic, A., Chaudhary, G., & Goia, F. (2021). Designing the design of experiments (DOE) – An investigation on the influence of different factorial designs on the characterization of complex systems. *Energy and Buildings, 250*, 111298. https://www.sciencedirect.com/science/article/pii/S037877882100582X

Li, Z., Xu, X., Zhang, S., Xie, S., Gao, Z., Zhao, J. …Hua, G., (2025). Orthogonal experiment-based optimization of FWSF CW design parameters for enhanced hydraulic and treatment performance. *Desalination and Water Treatment, 324*, 101506. https://www.sciencedirect.com/science/article/pii/S1944398625005223

Patton, J., Periaswamy, S., Dunn, L., & McDaniel, A. L. (2023*). Retail case studies 2023 survey of retail industry innovation*. Auburn University RFID Lab. https://rfid.auburn.edu/papers/pages/2023RetailInnovationsDART.php?utm_source=RFID&utm_medium=web

Paul, A (2020). *Design of Experiments for 21st Century Engineers, The Fastest way to find out!* (1st ed.). United Kingdom: www.Lulu.com

Schmidt, S. R., & Launsby, R. G. (1994). *Understanding Design of Experiments.* Air Academy Press. https://airacad.com/books/understanding-industrial-designed-experiments/

Trotta, S., Binda, G., Ferrario, M. F., Pozzi, A., & Michetti, A. M. (2026). A Design of Experiment Approach to Arsenic Retention: Interactions between Sediment Properties and Water Chemistry. *Journal of Hazardous Material Advances, 21*, 100977. https://www.sciencedirect.com/science/article/pii/S2772416625003882?via%3Dihub

Biographies

RAJESH BALASUBRAMANIAN is an assistant professor at the University of Memphis. He worked in industry for over 27 years before accepting a teaching position. He has been teaching quality control, facility design, and project planning to undergraduate students. Given his industrial background, he works on statistical analysis and data presentation in the RFID space. Mr. Balasubramanian may be reached at rbalasub@memphis.edu

KEVIN BERISSO is the Director of the AutoID Lab at the University of Memphis. He has been teaching within the AutoID industry for over 20 years, is a member of the AIDC 100, and received the Ted Williams award by AIM Inc. for his work in industry. He is a regular presenter at RFID Journal Live and has worked with GS1 on barcode research, as well as being involved in RFID research for returnable transport items in the automotive industry and tagging items in the aerospace industry. Dr. Berisso may be reached at kberisso@memphis.edu

Enhancing Public Awareness of Invasive Species Through an AR-Enabled Dodecahedron

Michael Dakeev, Sam Houston State University; Autumn Smith-Herron, Sam Houston State University

Abstract

From this study, the authors present their version of an augmented reality (AR) educational installation designed to improve public awareness of invasive beetle species. The system combined a physical dodecahedron structure with interactive AR visualizations created in Unity, a real-time 3D development engine. Each face of the dodecahedron displays information about different invasive species, while allowing users to scan the panels to view 3D beetle models and animations in AR. The dodecahedron structure naturally draws attention, encourages curiosity, and promotes hands-on interaction across different age groups, including retirees. To evaluate usability and engagement, a questionnaire with ten Likert-scale questions, focusing on visual appeal, interactivity, realism, and educational values was prepared. Data were collected and analyzed to evaluate how AR and tangible design increased interest and knowledge retention. The goal of this project was to demonstrate that combining physical exhibits with AR content can create accessible and immersive learning experiences in visitor centers and educational environments. The aim of this approach was to make scientific topics, such as invasive species, more understandable and engaging for the general public.

Introduction

Invasive species pose significant ecological and economic challenges, making public awareness and education critical components of prevention and mitigation strategies. Visitor centers, outreach events, and informal learning environments provide valuable opportunities to engage the public; however, traditional static displays often struggle to effectively capture attention or convey complex ecological dynamics. Augmented reality (AR) has emerged as a promising approach for enhancing informal learning by combining interactive digital content with physical artifacts, allowing users to visualize complex systems, explore cause-effect relationships, and engage with educational material in an immersive manner (Azuma, 1997; Dakeev, Pecen, Yildiz, Basith & Khan, 2023; Dede, 2014; Ibáñez & Delgado-Kloos, 2018; Johnson et al., 2024).

To support invasive species outreach, a physical AR Station was developed that integrated a dodecahedron-shaped device with an AR experience, featuring three-dimensional models, interactive elements, and simulation-based content related to the impacts of invasive species. Figure 1 shows how the design emphasized intuitive interaction, visual appeal, and immersion, with the goal of increasing user engagement while improving understanding of the ecological consequences of invasive species and the importance of public awareness (Dakeev & Aljaroudi, 2022; Dakeev, Pecen, Yildiz, Sowell, Obeidat & Basith, 2022).

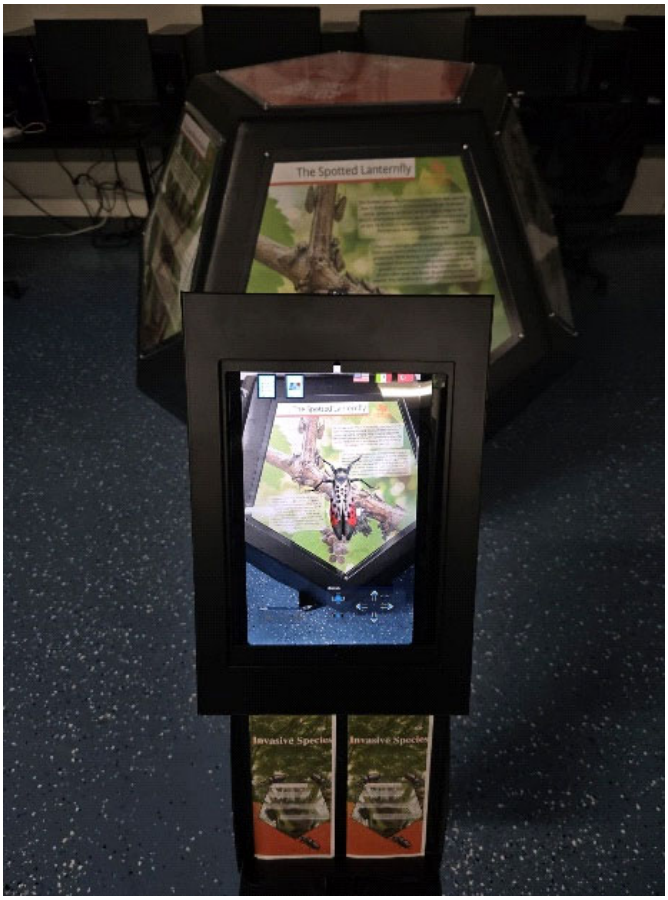

Figure 1. AR application interaction with invasive species information.

The purpose of this study was to evaluate user perceptions of the AR Station and to identify the design factors that contributed most strongly to its outreach effectiveness. Specifically, the authors examined how users rated the usability of the interface, the level of engagement and immersion provided by the experience, and the perceived educational value of the AR content. In addition, the authors investigated whether these perceptions varied across different visitor groups interacting with the AR Station under varying deployment conditions. Groups corresponded to separate deployment sessions/cohorts. Finally, the authors explored which aspects of the user experience—immersion, realism of the AR models, perceived usefulness of the data

and simulation components, etc.—were most strongly associated with users' willingness to tell others about invasive species and the AR application, a key indicator of outreach amplification. Prior work has shown that immersive AR and VR experiences can positively influence motivation, engagement, and spatial understanding, suggesting that well-designed AR systems may enhance outreach effectiveness in informal learning contexts from kindergarten to college-level education (Dakeev, Obeidat, Demiroz & Lombardo, 2026; Dakeev & Aljaroudi, 2022; Clint, Dakeev, Pecen & Yildiz, 2020; Makransky, Andreasen, Baceviciute & Mayer, 2021; Slater & Wilbur, 1997).

Participants and Data

Data for this study were collected using a post-experience survey administered to participants after they interacted with the AR Station. Figure 2 shows how the AR Station was deployed in an informal outreach setting, where visitors were invited to explore the augmented reality content independently or with minimal facilitation. Upon completion of the experience, participants were asked to complete a brief, anonymous survey evaluating their interaction with the system. A total of 238 valid survey responses were collected across six distinct visitor groups representing separate deployment sessions of the AR Station. These groups did not correspond to demographic categories, but rather to different outreach events and implementation contexts, which may have varied in factors such as facilitation style, crowd density, and user interaction conditions. One respondent did not specify group affiliation and was included in aggregate analyses but excluded from group-based comparisons.

Figure 3 shows a case of a user responding to the survey instrument that consisted of ten Likert-scale items rated on a five-point scale, where higher values indicated more positive perceptions. Likert-scale survey instruments are commonly used in user experience and educational technology research; however, such data are ordinal in nature and require appropriate analytical treatment (Lionello, Aletta, Mitchell & Kang, 2021). The items assessed multiple aspects of the AR Station experience, including interface intuitiveness, engagement, visual appeal of the device, perceived impact of invasive species, importance of public awareness, realism of the AR models, usefulness of the dodecahedron form factor, usefulness of the data or simulation components, overall immersion, and likelihood of telling others about invasive species and the AR application. An optional open-ended comment field was included to capture qualitative feedback and suggestions for improvement. All responses were collected electronically and exported to a spreadsheet format for analysis. No personally identifiable information was recorded, and participation was voluntary. The study design focused on capturing immediate user perceptions following interaction with the AR Station to evaluate usability, engagement, and perceived outreach effectiveness in a realistic deployment context.

Figure 2. Student interaction with the campus community.

Figure 3. Survey Questionnaire for Public Education/Awareness on Invasive Species

Data Collection and Analysis

Survey responses were exported to a spreadsheet and analyzed using statistical techniques appropriate for ordinal data. Descriptive statistics (mean and standard deviation)

were calculated to summarize user perceptions. The internal consistency of the survey instrument was assessed using Cronbach's alpha coefficient to evaluate whether the set of items reliably measured a cohesive user experience construct. To examine the underlying structure of the survey, a principal component analysis was conducted to determine whether the items reflected a dominant overall experience factor or multiple distinct dimensions. Differences in user perceptions across visitor groups were evaluated using the Kruskal–Wallis test (Kruskal & Wallis, 1952), which is well suited for Likert-scale data and does not assume normality. When statistically significant group effects were identified, post-hoc pairwise comparisons were performed to explore which groups differed meaningfully from one another.

Finally, to investigate which aspects of the AR Station experience were most strongly associated with outreach amplification, predictive modeling was performed using ordinary least squares regression. In this analysis, participants' likelihood of telling others about invasive species and the AR application served as the outcome variable, while selected experience-related survey items were used as predictors. Although Likert-scale data impose limitations on strict causal interpretation, the regression analysis was used to identify directional relationships and to highlight experience factors with the greatest practical influence on user willingness to share the experience.

Results

Descriptive statistics were reported as mean (M), standard deviation (SD), and sample size (N). Overall, participants rated the AR Station very positively across all measured dimensions. Mean ratings for the ten survey items ranged from 4.50 to 4.77 on a five-point scale, indicating consistently high levels of perceived usability, engagement, and educational value. Table 1 indicates that participants reported highly positive perceptions of usability, engagement, and visual appeal, as well as strong ratings related to learning and awareness of invasive species. Items associated with the AR experience were also rated highly. Participants reported strong perceptions of model realism, usefulness of the dodecahedron form, and the value of data and simulation components. Immersion and likelihood of telling others showed slightly greater variability compared to other measures, suggesting more differentiation in user responses for these outcomes.

Table 2 shows that the ten Likert-scale items demonstrated excellent internal consistency, with a Cronbach's alpha of 0.913, indicating that the instrument reliably captured a cohesive perception of the AR Station experience. The internal consistency of the survey instrument was assessed using Cronbach's alpha, a widely accepted measure for evaluating the reliability of multi-item scales (Cronbach, 1951). To further examine the underlying structure of the survey, principal component analysis was conducted. Results indicated a dominant first principal component accounting for approximately 57% of the total variance, consistent with the presence of a strong overall positive experience or perceived impact factor rather than multiple unrelated constructs.

Table 2. Reliability statistics for AR Station survey items.

Cronbach's alpha	N of Items
0.913	10

Table 1. Descriptive statistics.

Descriptive Statistics					
	N	Minimum	Maximum	Mean	Std. Deviation
Intuitive interface controls	238	1	5	4.769	0.560
Engagement	238	1	5	4.710	0.626
Visual appeal	238	1	5	4.735	0.631
Perceived invasive species impact	238	1	5	4.697	0.657
Importance of public awareness	238	1	5	4.752	0.604
AR model realism	238	1	5	4.609	0.725
Dodecahedron usefulness	238	1	5	4.655	0.655
Data/simulation usefulness	238	1	5	4.718	0.610
Immersion	238	1	5	4.576	0.822
Likelihood to tell others	238	1	5	4.500	0.889
Valid N (listwise)	238				

Table 3 summarizes the results of the Kruskal–Wallis analysis for all survey items. Differences in user perceptions across visitor groups were examined using the Kruskal–Wallis test. Statistically significant group effects were observed for perceived intuitiveness of the user interface ($\chi^2(5) = 22.57$, $p < 0.001$) and likelihood of telling others about the AR application and invasive species ($\chi^2(5) = 13.51$, $p = 0.019$). For interface intuitiveness, Group 6 reported the lowest mean rating ($M = 4.28$), while several other groups reported higher means, including Group 3 ($M = 4.90$) and Group 1 ($M = 4.84$). Post-hoc pairwise comparisons with correction indicated that Group 6 differed most clearly from Groups 1 through 3 on this measure. No statistically significant differences were detected for the remaining survey items ($p > 0.05$), though several measures exhibited trend-level effects. Principal component analysis is commonly used to explore whether survey instruments reflect a dominant underlying construct or multiple dimensions in exploratory evaluation studies (Sam et al., 2018).

Statistically significant group differences were observed for perceived intuitiveness of the interface ($\chi^2(5) = 22.57$, $p < 0.001$) and likelihood of telling others about the AR application ($\chi^2(5) = 13.51$, $p = 0.019$). These differences suggest that contextual factors such as facilitation style, crowding, device availability, or brief variations in onboarding or instruction across deployment sessions may influence perceived usability. Importantly, these findings point to actionable opportunities for improving consistency in future deployments through standardized onboarding and facilitation practices.

To identify experience factors most strongly associated with outreach amplification, correlations and regression analyses were conducted using the participants' likelihood of telling others as the outcome variable. Prior research demonstrated that immersion, realism, and meaningful interaction are key drivers of engagement and learning outcomes in immersive technologies (Makransky et al., 2021; Slater & Wilbur, 1997). Participant willingness to tell others was measured using the survey item "Likelihood to tell others about invasive species and the AR application" (Q10). A Spearman correlation analysis revealed strong positive associations between willingness to tell others and several experience-related measures, particularly overall immersion usefulness of the data or simulation components, usefulness of the dodecahedron form factor, and realism of the AR models.

A multiple regression model using key experience variables explained a substantial portion of the variance in willingness to tell others ($R^2 = 0.509$). Within this model, immersion emerged as the strongest predictor, followed by model realism and perceived usefulness of the data or simulation components. These results indicated that participants were more likely to share the experience when the AR interaction felt immersive, visually and behaviorally realistic, and supported by meaningful informational or simulation content.

Discussion

The results of this study indicated that the AR Station effectively achieved its primary goals of usability, engagement, and educational outreach. Participants consistently rated the interface controls as intuitive, the interaction as engaging, and the physical device as visually appealing. These uniformly high ratings suggested that users were able to interact with the system with minimal friction, allowing them to focus on the content rather than on learning how to operate the technology. Moreover, the high rating for the perceived importance of public awareness of invasive species underscored that the AR Station successfully aligned technological novelty with a meaningful educational

Table 3. Kruskal-Wallis analysis of survey items by AR Station group.

Item	χ^2 (H)	df	p-value	Interpretation
Q1 – Intuitive interface controls	22.567	5	< 0.001	Significant
Q2 – Engagement	3.848	5	0.572	n.s.
Q3 – Visual appeal	9.482	5	0.091	n.s. (trend)
Q4 – Perceived invasive species impact	2.808	5	0.730	n.s.
Q5 – Importance of public awareness	9.592	5	0.088	n.s. (trend)
Q6 – AR model realism	6.100	5	0.297	n.s.
Q7 – Dodecahedron usefulness	9.747	5	0.083	n.s. (trend)
Q8 – Data / simulation usefulness	7.508	5	0.186	n.s.
Q9 – Immersion	7.977	5	0.158	n.s.
Q10 – Likelihood to tell others	13.505	5	0.019	Significant

Note: n.s. = not significant. Trend indicates $0.05 \leq p \leq 0.10$.

mission, rather than being perceived as technology deployed for its own sake. This alignment is critical for outreach-oriented applications, where sustained attention and message retention are central objectives.

Beyond overall satisfaction, the modeling results provided insight into which aspects of the experience most strongly influenced user willingness to share the information with others. Immersion emerged as the most influential factor, followed closely by the realism of the AR models and the perceived usefulness of the data or simulation components. These findings suggest that outreach effectiveness is maximized when users feel absorbed in the experience, perceive the virtual content as realistic and credible, and clearly understand how the interactive data or simulations contribute to learning. Design efforts that prioritize immersion and realism are therefore likely to yield the greatest gains in outreach amplification. At the same time, this finding highlights an important consideration: highly immersive technologies may also increase the persuasive impact of presented content, regardless of its accuracy. This underscores the importance of ensuring that AR-based educational experiences are grounded in scientifically validated information and carefully designed to support accurate interpretation, particularly when engaging general audiences.

Several specific design implications emerged from these findings. Reducing interaction friction—such as improving tracking stability, minimizing load times, and shortening the path to the initial "wow" moment—can enhance immersion and sustain user engagement. Incorporating short narrative sequences that guide users through stages of observation, identification, impact, and action may further strengthen the educational arc of the experience. Improvements to model fidelity, including enhanced lighting, shadows, scale cues, and animation, can increase perceived realism and reinforce user trust in the content. In addition, making the value of the data or simulation components more explicit through concise visual callouts or a brief summary panel at the conclusion of the experience may help users better articulate what they learned and why it matters, thereby increasing their likelihood of sharing the experience with others.

The group-level differences observed in perceived interface intuitiveness and willingness to tell others highlight the importance of consistent deployment practices. Variations in facilitation, onboarding, crowding, or device availability may influence user perceptions even when the underlying technology remains the same. Providing a standardized onboarding script or clearly visible instructional signage, along with tracking facilitator presence and approximate time-on-task, may help reduce variability across deployments and improve consistency in user experience. Several limitations of this study should be acknowledged. The high overall ratings across most survey items indicate the presence of a ceiling effect, which may limit sensitivity to smaller differences among participants or design variations.

Additionally, the evaluation was conducted using a single instrument in a specific deployment context, and future studies involving additional sites and audiences are needed to establish broader generalizability. Finally, the results rely on self-reported perceptions rather than objective performance or learning measures. Future work could strengthen evaluation by incorporating behavioral metrics such as time-on-task, interaction completion rates, or pre- and post-experience knowledge assessments to complement subjective user feedback. These findings align with prior AR and MR (mixed-reality) research demonstrating that immersive, well-designed interactive systems can improve engagement, learning, and user motivation across educational and training contexts (Dakeev & Aljaroudi, 2022; Dakeev et al., 2022; Ibáñez & Delgado-Kloos, 2018). This reinforces theoretical frameworks that emphasize immersion and presence as central mechanisms through which virtual and augmented environments influence user behavior and learning (Makransky et al., 2021; Slater & Wilbur, 1997).

Conclusions

In this study, the authors demonstrated that a dodecahedron-based AR Station can achieve strong usability and engagement while supporting invasive species outreach objectives. Survey results from 238 participants showed consistently high ratings and excellent instrument reliability. Group comparisons indicated that session-level implementation factors can measurably affect perceived intuitiveness and willingness to share. Most importantly, immersion, AR model realism, and perceived usefulness of data and simulation components are key drivers of user willingness to tell others, offering clear priorities for iterative improvement and scaling.

Acknowledgements

This work was supported by the U.S. Department of Agriculture, Animal and Plant Health Inspection Service (USDA/APHIS), with additional support from Sam Houston State University. The authors acknowledge the contributions of student research assistants and collaborating partner sites that supported fabrication, testing, and applied deployment activities.

References

Azuma, R. T. (1997). A survey of augmented reality. *Presence: Teleoperators and Virtual Environments*, *6*(4), 355-385. https://doi.org/10.1162/pres.1997.6.4.355

Clint, E., Dakeev, U., Pecen, R., & Yildiz, F. (2020). *Effect of an augmented reality tool in early student motivation and engagement* [Conference presentation]. CIEC Conference, Orlando, Florida. https://doi.org/10.18260/1-2-370-38705

Cronbach, L. J. (1951). Coefficient alpha and the internal structure of tests. *Psychometrika*, *16*(3), 297-334. https://doi.org/10.1007/BF02310555

Dakeev, M., Obeidat, S., Demiroz, F., & Lombardo, V. (2026). Augmented reality in foot palpation: Enhancing accuracy and training medial cuneiform bone localization. Zenodo repository. https://doi.org/10.5281/zenodo.18380510

Dakeev, U., & Aljaroudi, A. (2022). Innovative augmented reality (AR) application for effective utilization of hazard communication pictograms. *International Journal of Engineering Research and Innovation*, *14*(1), 29-32.

Dakeev, U., Pecen, R., Yildiz, F., Basith, I., Khan, V., Rabe, C. J. …Sowell, L. E. (2023). *A feasibility study of spatial cognition assessment in virtual reality for computer aided design students* [Conference presentation]. ASEE Annual Conference and Exposition Proceedings, Baltimore, Maryland. https://doi.org/10.18260/1-2--42390

Dakeev, U., Pecen, R., Yildiz, F., Sowell, L., Obeidat, S., & Basith, I. (2022). *Development of virtual reality robotics laboratory simulation* [Conference presentation]. ASEE Zone IV Conference. https://aseezoneiv2022.engineering.ubc.ca/

Dede, C. (2014). The role of digital technologies in deeper learning. Jobs for the Future. https://files.eric.ed.gov/fulltext/ED561254.pdf

Ibáñez, M.-B., & Delgado-Kloos, C. (2018). Augmented reality for STEM learning: A systematic review. *Computers & Education*, *123*, 109-123. https://doi.org/10.1016/j.compedu.2018.05.002

Johnson, M., Lavi, R., De Weck, O., Hajela, P., Carlone, L., Hu, S. …Chang, Y. (2024). *A comparative study of the impact of virtual reality on student learning and satisfaction in aerospace education* [Conference presentation]. ASEE Annual Conference and Exposition Proceedings, Portland, Oregon. https://doi.org/10.18260/1-2--46426

Kruskal, W. H., & Wallis, W. A. (1952). Use of ranks in one-criterion variance analysis. *Journal of the American Statistical Association*, *47*(260), 583-621. https://doi.org/10.1080/01621459.1952.10483441

Lionello, M., Aletta, F., Mitchell, A., & Kang, J. (2021). Introducing a method for intervals correction on multiple Likert scales: A case study on an urban soundscape data collection instrument. *Frontiers in Psychology*, *11* (2020), 602831. https://doi.org/10.3389/fpsyg.2020.602831

Makransky, G., Andreasen, N. K., Baceviciute, S., & Mayer, R. E. (2021). Immersive virtual reality increases liking but not learning with a science simulation and generative learning strategies promote learning in immersive virtual reality. *Journal of Educational Psychology*, *113*(4), 719-735. https://doi.org/10.1037/edu0000473

Sam, A. H., Field, S. M., Collares, C. F., Van Der Vleuten, C. P. M., Wass, V. J., Melville, C. …Meeran, K. (2018). Very short-answer questions: Reliability, discrimination and acceptability. *Medical Education*, *52* (4), 447-455. https://doi.org/10.1111/medu.13504

Slater, M., & Wilbur, S. (1997). A framework for immersive virtual environments (FIVE): Speculations on the role of presence in virtual environments. *Presence: Teleoperators and Virtual Environments*, *6*(6), 603-616. https://doi.org/10.1162/pres.1997.6.6.603

Biographies

MICHAEL U. DAKEEV is an associate professor and program coordinator of the Engineering Design Technology Program at Sam Houston State University. He holds a PhD in Technology, an MS in Industrial Management, and a BS in Industrial Engineering. Dr. Dakeev's work focuses on applied engineering education, certification training, and immersive learning through AR/VR tools. Dr. Dakeev may be reached at dakeev@shsu.edu

AUTUMN J. SMITH-HERRON is the Director of Innovative Research and Collaborative Programs in the Office of Research and Sponsored Programs at Sam Houston State University. She also serves as Co-Editor-in-Chief of Comparative Parasitology. Dr. Smith-Herron's work focuses on advancing interdisciplinary research initiatives, fostering external partnerships, and supporting technology-driven educational and outreach programs. Dr. Smith-Herron may be reached at smith-herron@shsu.edu

INSTRUCTIONS FOR AUTHORS: MANUSCRIPT FORMATTING REQUIREMENTS

The INTERNATIONAL JOURNAL OF ENGINEERING RESEARCH AND INNOVATION is an online/print publication designed for Engineering, Engineering Technology, and Industrial Technology professionals. All submissions to this journal, submission of manuscripts, peer-reviews of submitted documents, requested editing changes, notification of acceptance or rejection, and final publication of accepted manuscripts will be handled electronically. The only exception is the submission of separate high-quality image files that are too large to send electronically.

All manuscript submissions must be prepared in Microsoft Word (.doc or .docx) and contain all figures, images and/or pictures embedded where you want them and appropriately captioned. Also included here is a summary of the formatting instructions. You should, however, review the sample Word document on our website (http://ijeri.org/formatting-guidelines) for details on how to correctly format your manuscript. The editorial staff reserves the right to edit and reformat any submitted document in order to meet publication standards of the journal.

The references included in the References section of your manuscript must follow APA-formatting guidelines. In order to help you, the sample Word document also includes numerous examples of how to format a variety of scenarios. Keep in mind that an incorrectly formatted manuscript will be returned to you, a delay that may cause it (if accepted) to be moved to a subsequent issue of the journal.

1. **Word Document Page Setup:** Two columns with ¼" spacing between columns; top of page = ¾"; bottom of page = 1" (from the top of the footer to bottom of page); left margin = ¾"; right margin = ¾".

2. **Paper Title:** Centered at the top of the first page with a 22-point Times New Roman (Bold), small-caps font.

3. **Page Breaks:** Do not use page breaks.

4. **Figures, Tables, and Equations:** All figures, tables, and equations must be placed immediately after the first paragraph in which they are introduced. And, each must be introduced. For example: "Figure 1 shows the operation of supercapacitors." "The speed of light can be determined using Equation 4:"

5. **More on Tables and Figures:** Center table captions above each table; center figure captions below each figure. Use 9-point Times New Roman (TNR) font. Italicize the words for table and figure, as well as their respective numbers; the remaining information in the caption is not italicized and followed by a period—e.g., "*Table 1*. Number of research universities in the state." or "*Figure 5*. Cross-sectional aerial map of the forested area."

6. **Figures with Multiple Images:** If any given figure includes multiple images, do NOT group them; they must be placed individually and have individual minor captions using, "(a)" "(b)" etc. Again, use 9-point TNR.

7. **Equations:** Each equation must be numbered, placed in numerical order within the document, and introduced—as noted in item #4.

8. **Tables, Graphs, and Flowcharts:** All tables, graphs, and flowcharts must be created directly in Word; tables must be enclosed on all sides. The use of color and/or highlighting is acceptable and encouraged, if it provides clarity for the reader.

9. **Textboxes:** Do not use text boxes anywhere in the document. For example, table/figure captions must be regular text and not attached in any way to their tables or images.

10. **Body Fonts:** Use 10-point TNR for body text throughout (1/8" paragraph indention); indent all new paragraphs as per the images shown below; do not use tabs anywhere in the document; 9-point TNR for author names/affiliations under the paper title; 16-point TNR for major section titles; 14-point TNR for minor section titles.

11. **Personal Pronouns:** Do not use personal pronouns (e.g., "we" "our" etc.).

12. **Section Numbering:** Do not use section numbering of any kind.

13. **Headers and Footers:** Do not use either.

14. **References in the Abstract:** Do NOT include any references in the Abstract.

15. **In-Text Referencing:** For the first occurrence of a given reference, list all authors—last names only—up to seven (7); if more than seven, use "et al." after the seventh author. For a second citation of the same reference—assuming that it has three or more authors—add "et al." after the third author. Again, see the *sample Word document* and the *formatting guide for references* for specifics.

16. **More on In-Text References:** If you include a reference on any table, figure, or equation that was not created or originally published by one or more authors on your manuscript, you may not republish it without the expressed, written consent of the publishing author(s). The same holds true for name-brand products.

17. **End-of-Document References Section:** List all references in alphabetical order using the last name of the first author—last name first, followed by a comma and the author's initials. Do not use retrieval dates for websites.

18. **Author Biographies:** Include biographies and current email addresses for each author at the end of the document.

19. **Page Limit:** Manuscripts should not be more than 15 pages (single-spaced, 2-column format, 10-point TNR font).

20. **Page Numbering:** Do not use page numbers.

21. **Publication Charges:** Manuscripts accepted for publication are subject to mandatory publication charges.

22. **Copyright Agreement:** A copyright transfer agreement form must be signed by all authors on a given manuscript and submitted by the corresponding author before that manuscript will be published. Two versions of the form will be sent with your manuscript's acceptance email.

    Only one form is required. Do not submit both forms!

    The form named "paper" must be hand-signed by each author. The other form, "electronic," does not require hand signatures and may be filled out by the corresponding author, as long as he/she receives written permission from all authors to have him/her sign on their behalf.

23. **Submissions:** All manuscripts and required files and forms must be submitted electronically to Dr. Philip D. Weinsier, manuscript editor, at philipw@bgsu.edu.

24. **Published Deadlines:** Manuscripts may be submitted at any time during the year, irrespective of published deadlines, and the editor will automatically have your manuscript reviewed for the next-available issue of the journal. Published deadlines are intended as "target" dates for submitting new manuscripts as well as revised documents. Assuming that all other submission conditions have been met, and that there is space available in the associated issue, your manuscript will be published in that issue if the submission process—including payment of publication fees—has been completed by the posted deadline for that issue.

    Missing a deadline generally only means that your manuscript may be held for a subsequent issue of the journal. However, conditions exist under which a given manuscript may be rejected. Always check with the editor to be sure. Also, if you do not complete the submission process (including all required revisions) within 12 months of the original submission of your manuscript, your manuscript may be rejected or it may have to begin the entire review process anew.

THE LEADING JOURNAL OF ENGINEERING, APPLIED SCIENCE, AND TECHNOLOGY

Print ISSN: 2157-8052
Online ISSN: 1930-6628

www.ijme.us

www.iajc.org

INTERNATIONAL JOURNAL OF MODERN ENGINEERING

ABOUT IJME:

- IJME was established in 2000 and is the first and official flagship journal of the International Association of Journal and Conferences (IAJC).
- IJME is a high-quality, independent journal steered by a distinguished board of directors and supported by an international review board representing many well-known universities, colleges and corporations in the U.S. and abroad.
- IJME has an impact factor of **3.00**, placing it among the top 100 engineering journals worldwide, and is the #1 visited engineering journal website (according to the National Science Digital Library).

OTHER IAJC JOURNALS:

- The International Journal of Engineering Research and Innovation (IJERI)
  For more information visit www.ijeri.org
- The Technology Interface International Journal (TIIJ).
  For more information visit www.tiij.org

IJME SUBMISSIONS:

- Manuscripts should be sent electronically to the manuscript editor, Dr. Philip Weinsier, at philipw@bgsu.edu.

  For submission guidelines visit
  www.ijme.us/submissions

TO JOIN THE REVIEW BOARD:

- Contact the chair of the International Review Board, Dr. Philip Weinsier, at philipw@bgsu.edu.

  For more information visit
  www.ijme.us/ijme_editorial.htm

INDEXING ORGANIZATIONS:

- IJME is indexed by numerous agencies. For a complete listing, please visit us at www.ijme.us.

Contact us:

Mark Rajai, Ph.D.

Editor-in-Chief
California State University-Northridge
College of Engineering and Computer Science
Room: JD 4510
Northridge, CA 91330
Office: (818) 677-5003
Email: mrajai@csun.edu

www.tiij.org

www.ijeri.org

IJERI

The International Journal of Engineering Research & Innovation (IJERI) is the second official journal of the International Association of Journals and Conferences (IAJC). IJERI is a highly-selective, peer-reviewed print journal which publishes top-level work from all areas of engineering research, innovation and entrepreneurship.

IJERI Contact Information

General questions or inquiry about sponsorship of the journal should be directed to:

Mark Rajai, Ph.D.

Founding and Editor-In-Chief

Office: (818) 677-5003

Email: editor@ijeri.org

Department of Manufacturing Systems Engineering & Management

California State University-Northridge

18111 Nordhoff St.

Room: JD3317

Northridge, CA 91330